



Diagnostik von plasmabehandelten Oberflächen

H. Wulff
Universität Greifswald,
Institut für Chemie und Biochemie

Workshop

Mühlleithen , März 2006



1. Einführung

2. Methoden zur Analyse dünner Filme und Oberflächenschichten

Grazing incidence X-ray diffractometry GIXD

X-ray reflectometry, XR

XPS, AFM

3. Beispiele

3.1. Phasenanalyse

Ti-TiN_x HKBV

3.2. Defektstrukturanalyse

TiN_x Schichten, HKBV

3.3. Berechnung von Strukturgradienten

Ti films auf Si-Substraten HKBV

3.4. Untersuchung kinetischer Prozesse

ITO Schichten, DC Magnetron

3.5. Untersuchung von Clustern

Ag Cluster, DC Magnetron,
Gas-Aggregation Nanocluster Quelle

4. Zusammenfassung

Plasma
Energieeinstrom



Wand

$$Q_{in} = \int (J_{rad} + J_e + J_i + J_n + J_{ads} + J_{react} + J_{ext}) dA$$

Genotypus



Phänotypus

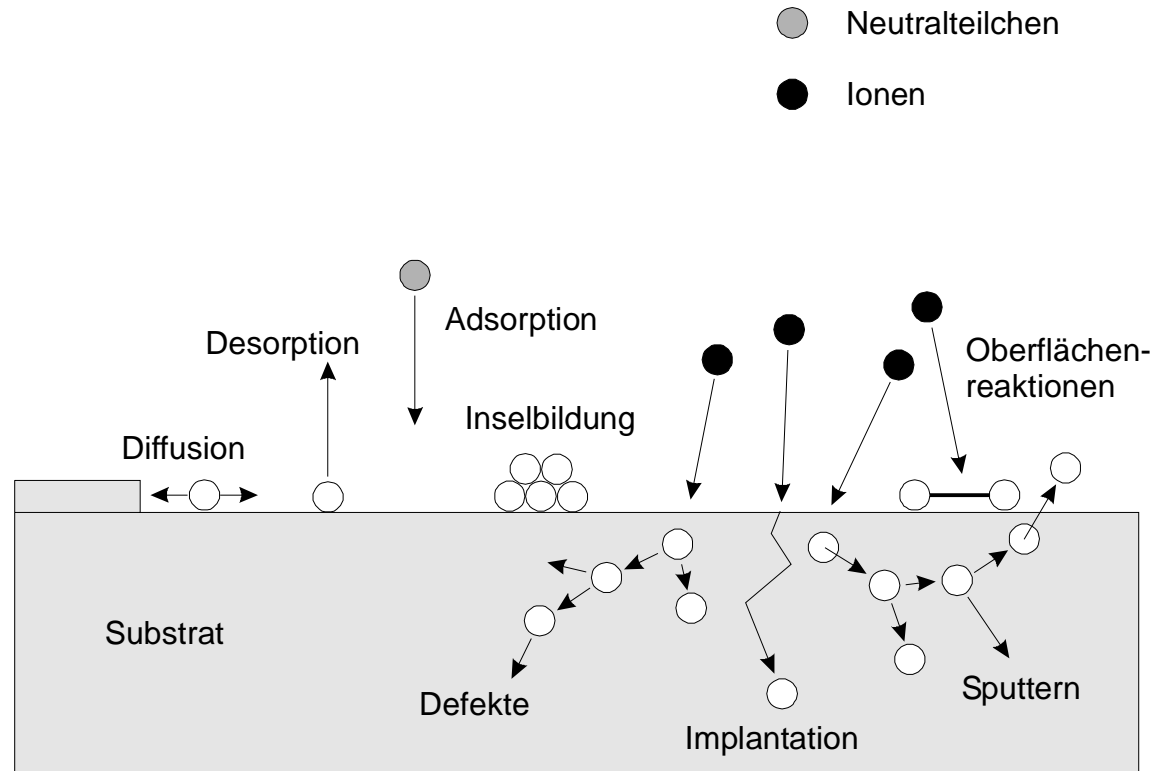
innerer Aufbau,
Struktur

korrespondierende
Gestalt, Verhalten,
Eigenschaften

Problem: Erklärungen aus ersten Prinzipien der Physik stehen noch aus

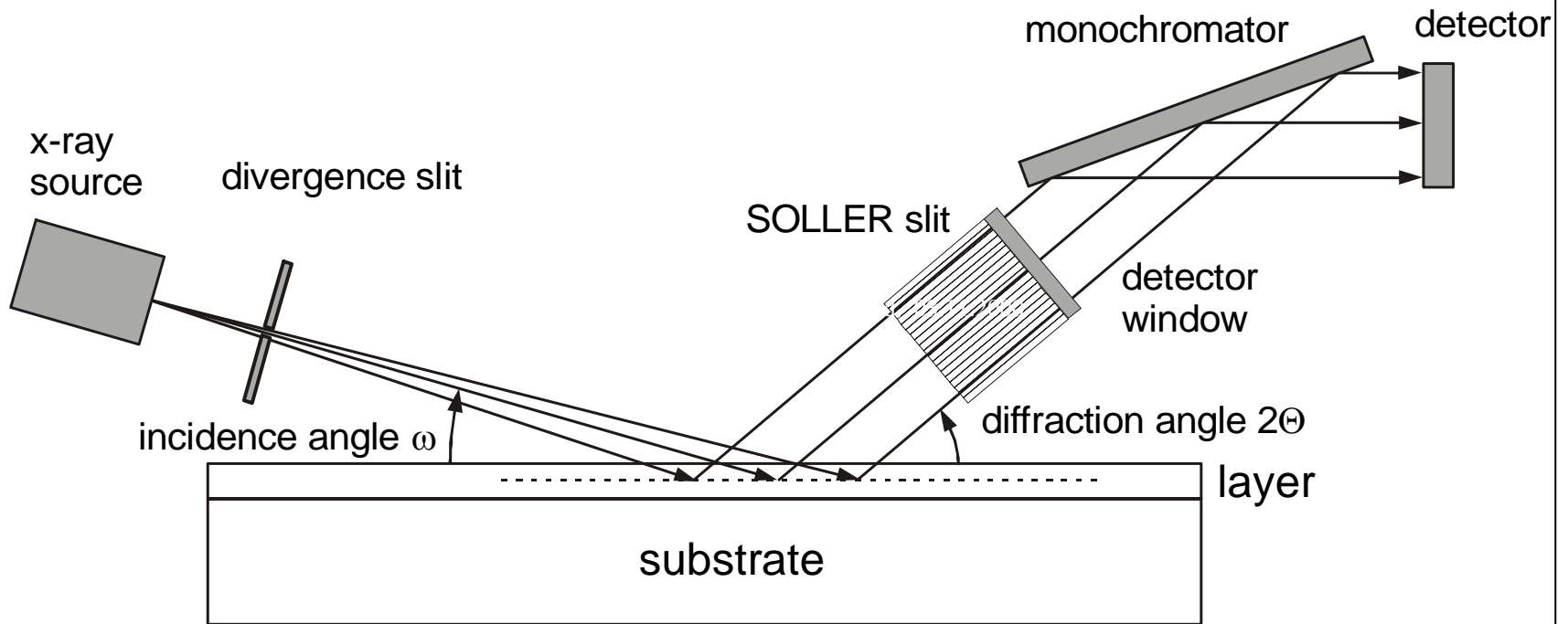
Wand:

Informationen in nm Bereich, Wirtiefe des Plasmas, zerstörungsfreie Untersuchungen

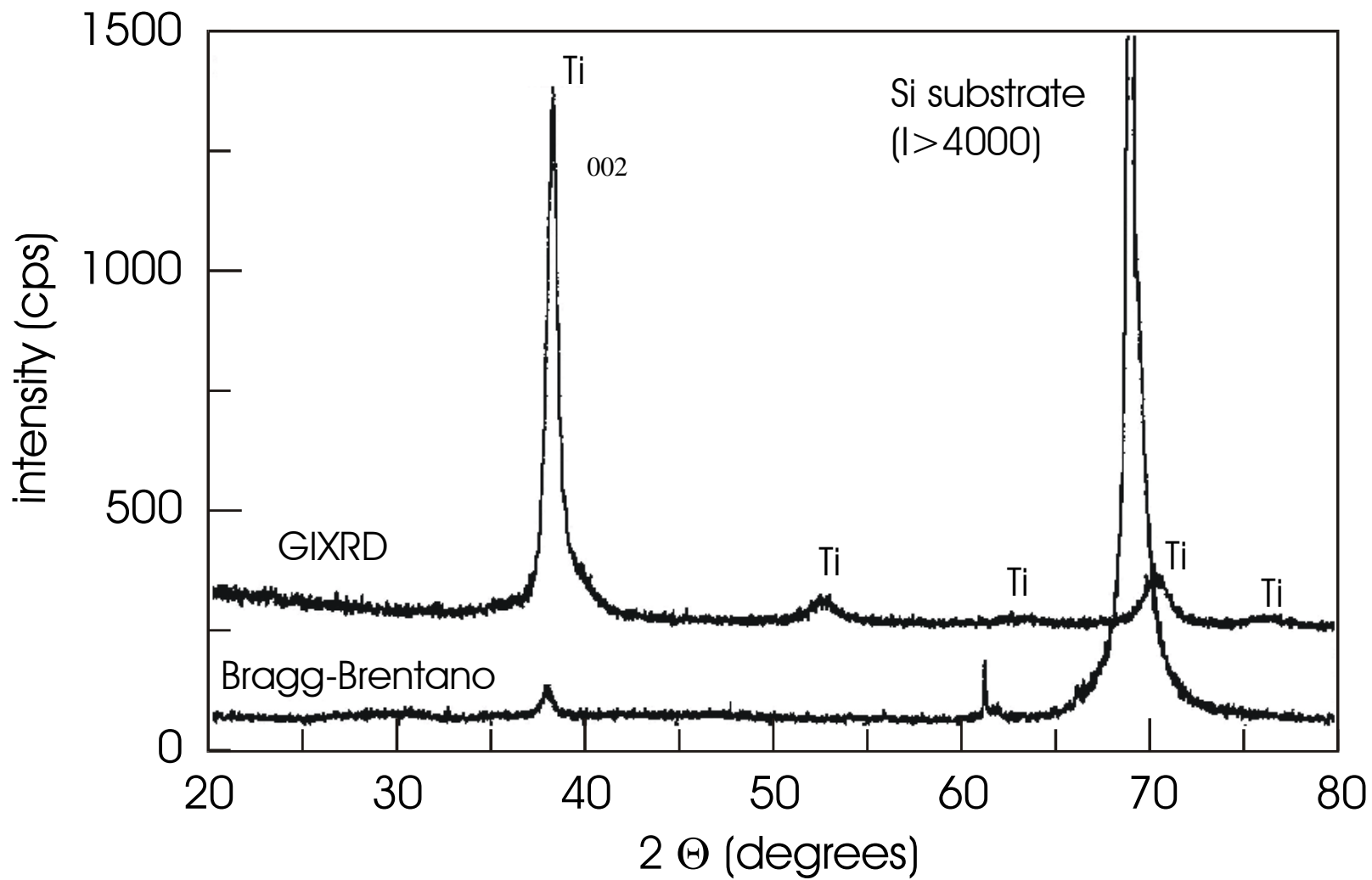


Model of plasma-wall-interactions

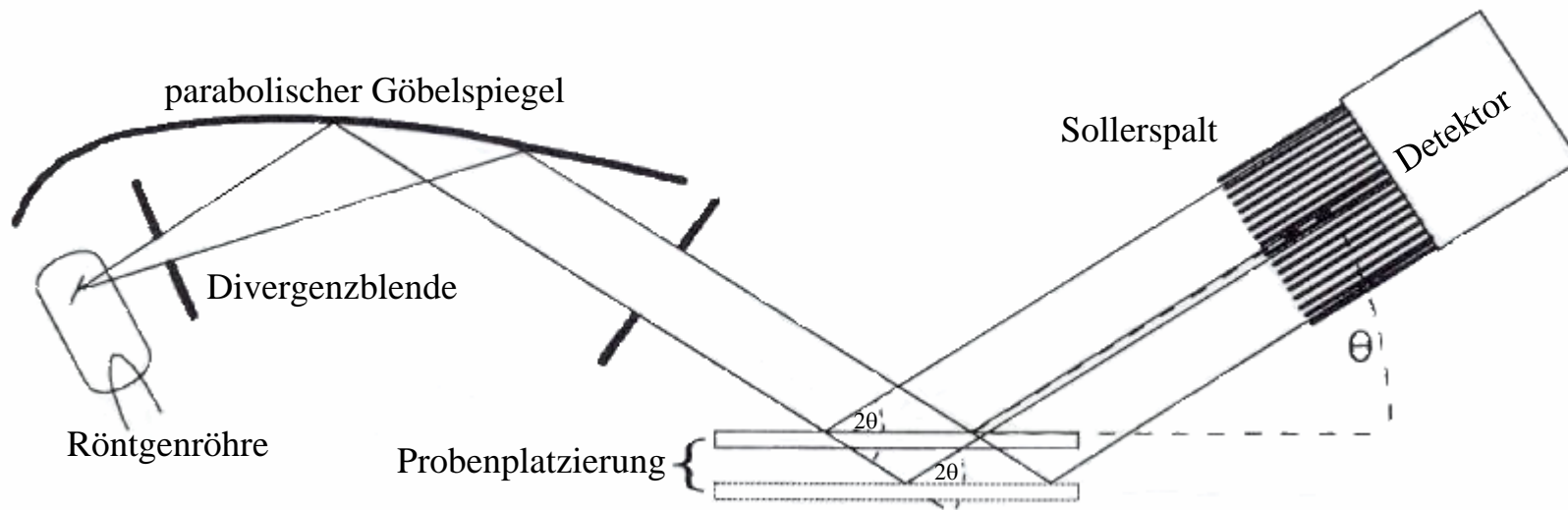
Film property	X-ray method	Alternatives
phase composition	GIXD : Bragg angle, intensity	TEM
chemical composition (mixed crystals)	GIXD : Bragg angle	EDX, XPS, RBS
macrostress	GIXD : Bragg angle	substrate curvature, laser optics
grain size	GIXD : line profile, line width	TEM, SEM
microstrain	GIXD : line profile	
preferred orientation	GIXD : intensity, polfigure	
crystal structure	GIXD : Rietveld analysis, structure refinement	
thickness	GIXD : intensity XR : Kiessig fringes	interferometry, ellipsometry, TEM
density	XR : critical angle of total reflection	ellipsometry
surface roughness interface roughness	XR : amplitude of Kiessig fringes	SEM, ellipsometry, AFM
diffusion behavior	in situ GIXD , thermal and time resolved: intensity	SIMS, AES, combined with sputtering
crystallization rate	in situ GIXD , thermal and time resolved: intensity	



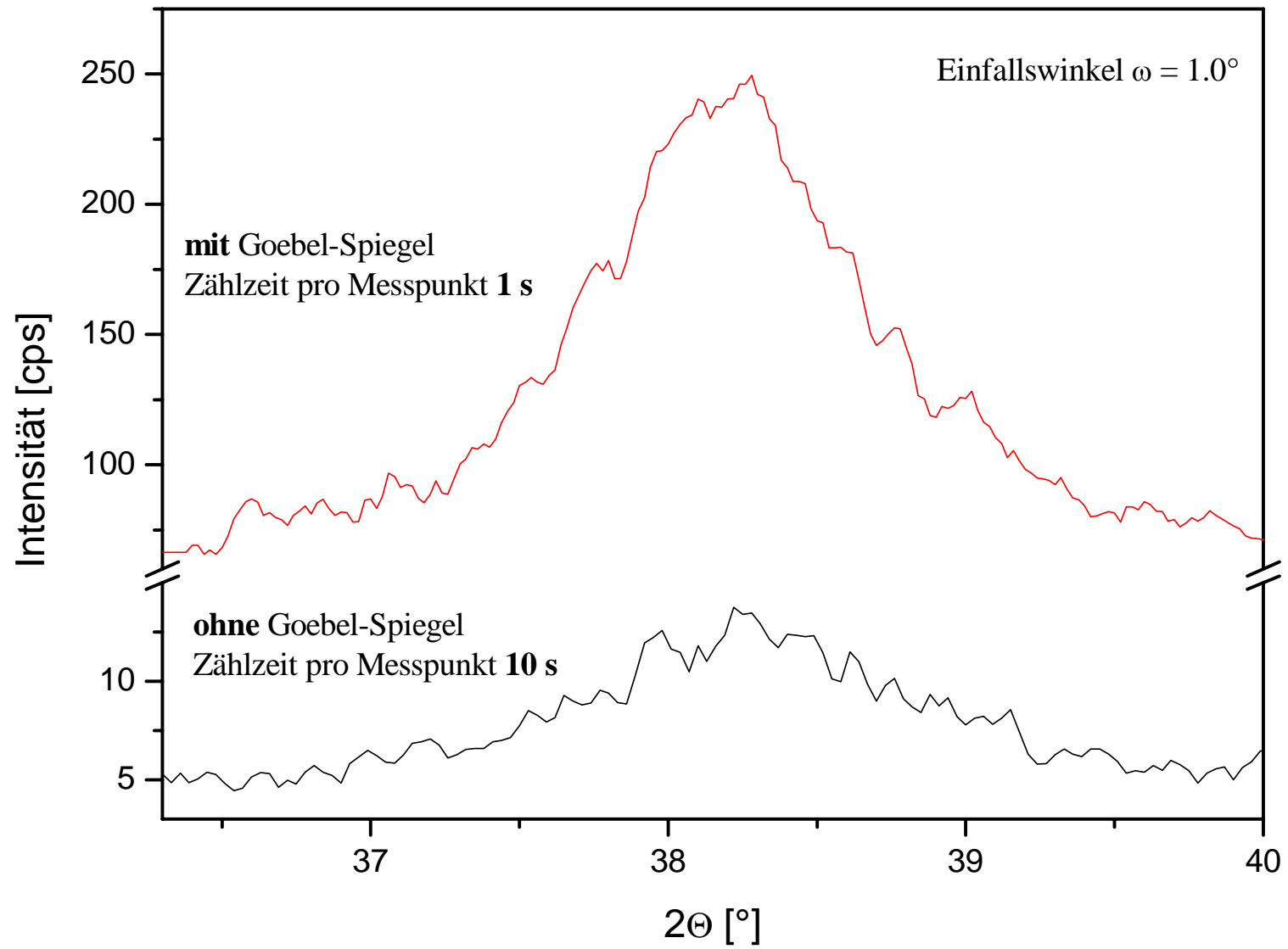
Schematic diagram of grazing incidence X-ray diffractometry (GIXD), 2θ Bragg angle, ω angle of incidence



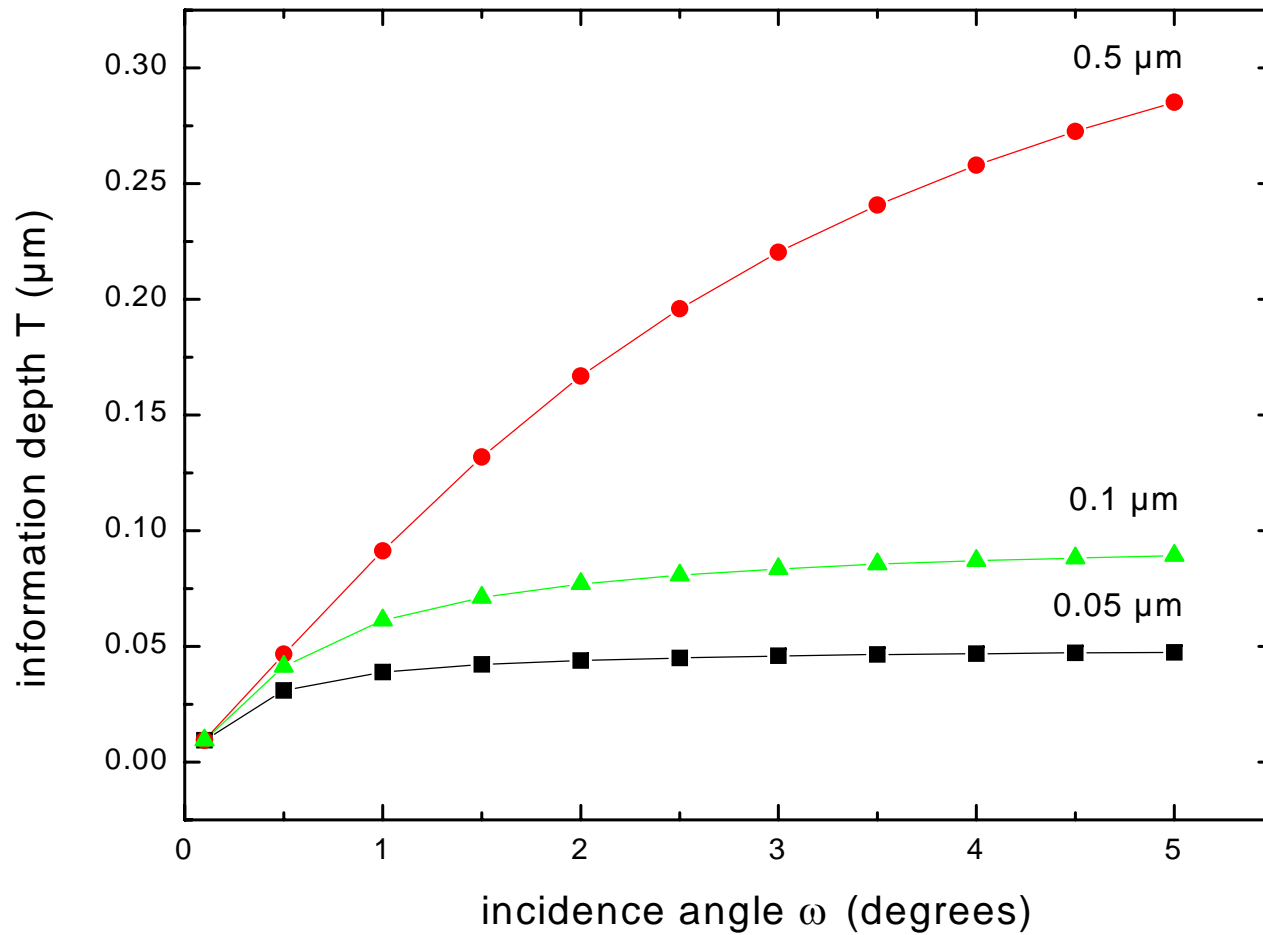
Advantage of GIXD-geometry for thin film investigations compared to conventional Bragg-Brentano measurement method



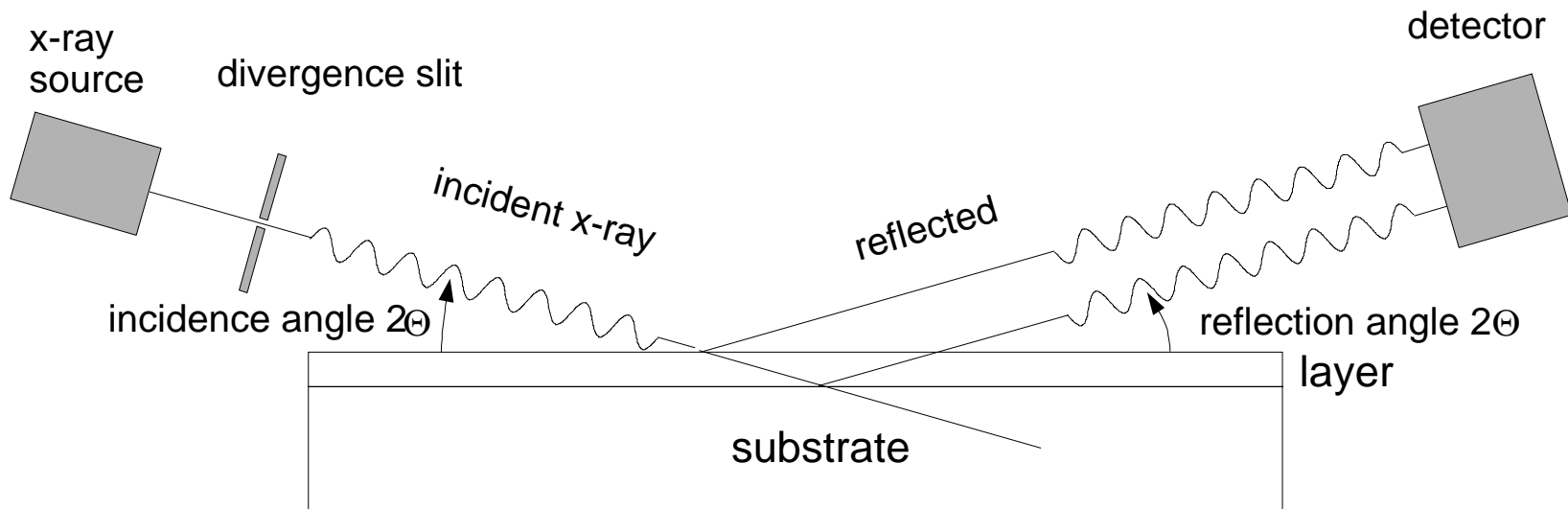
20 nm Silber auf Si-Wafer



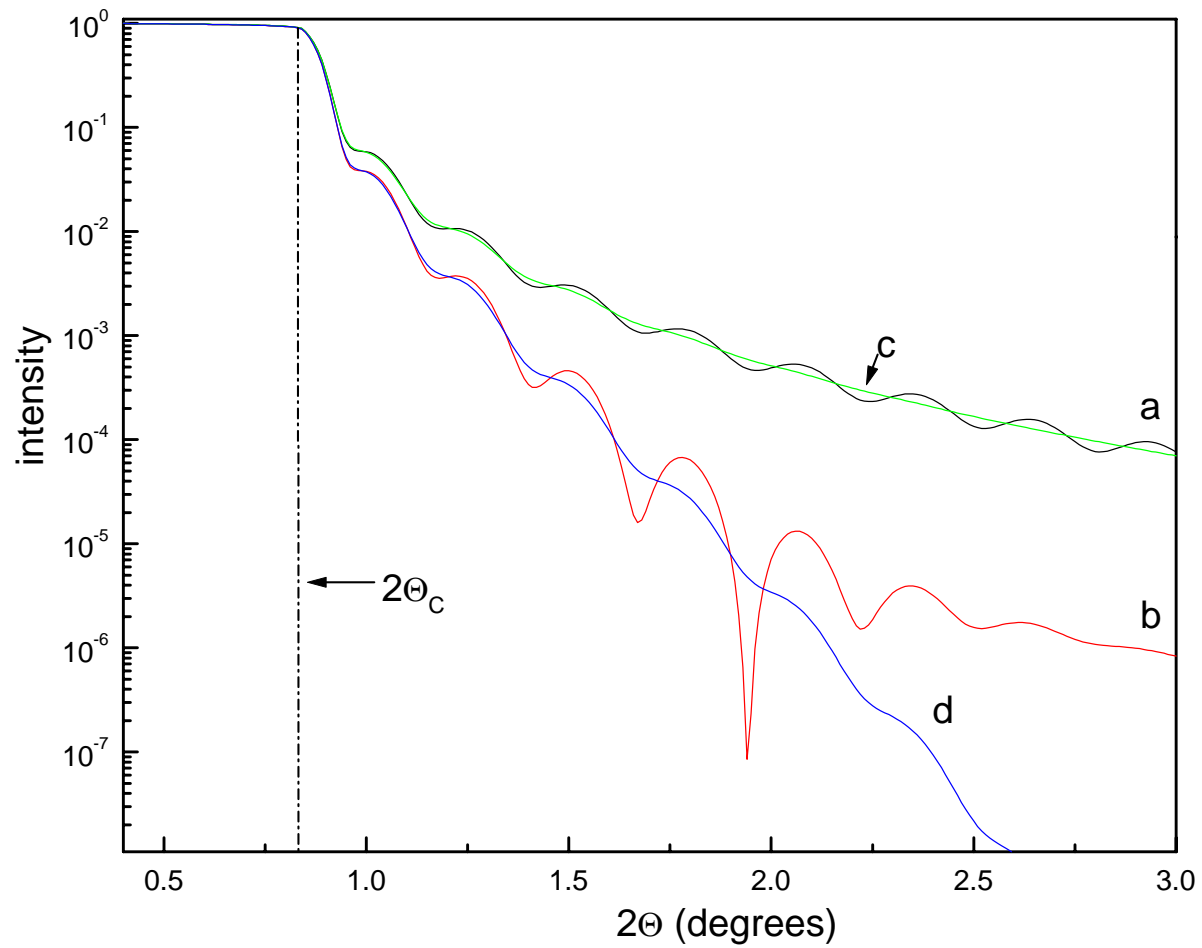
Kollimator 0.7°



Information depth of Cu K α radiation depending on incidence angles, calculated for 0.05, 0.1 and 0.5 μ m thick In films



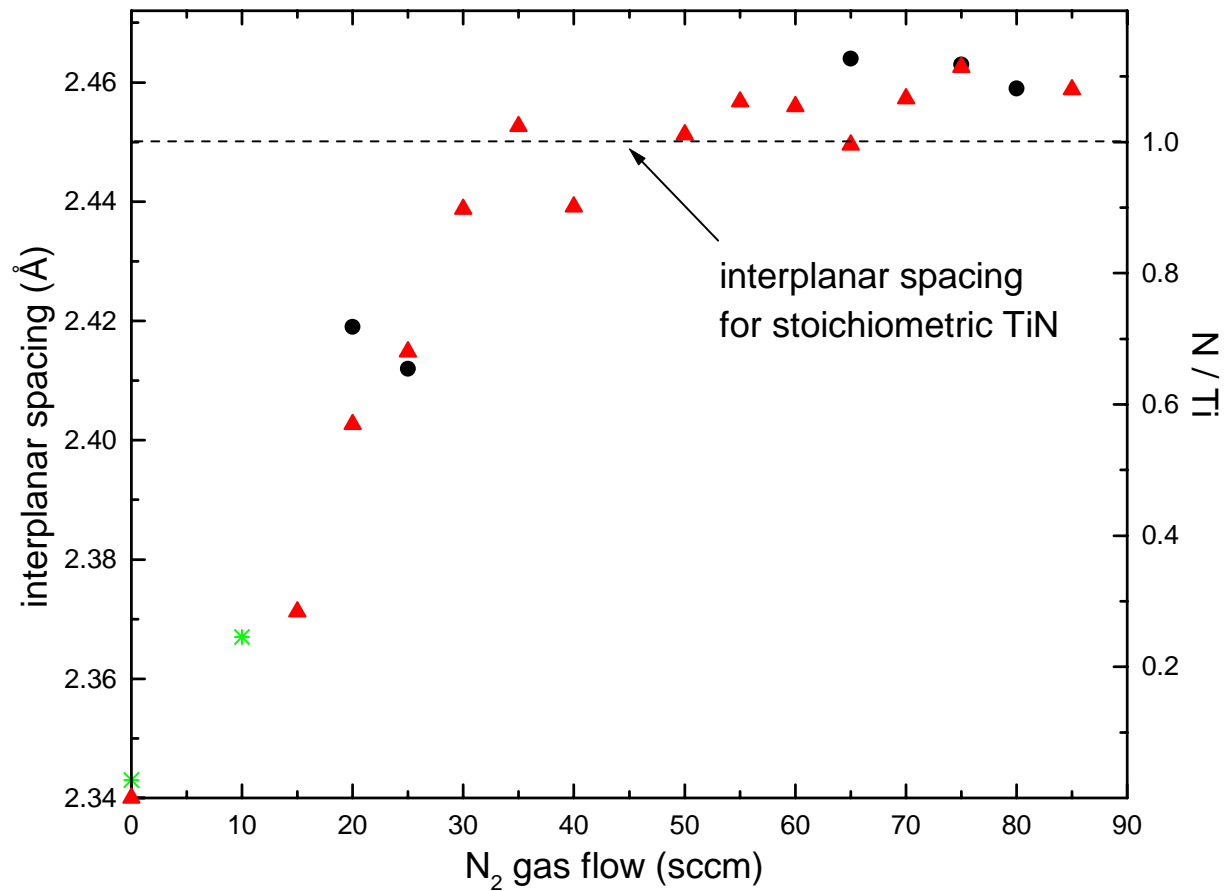
Schematic diagram of X-ray reflectometry



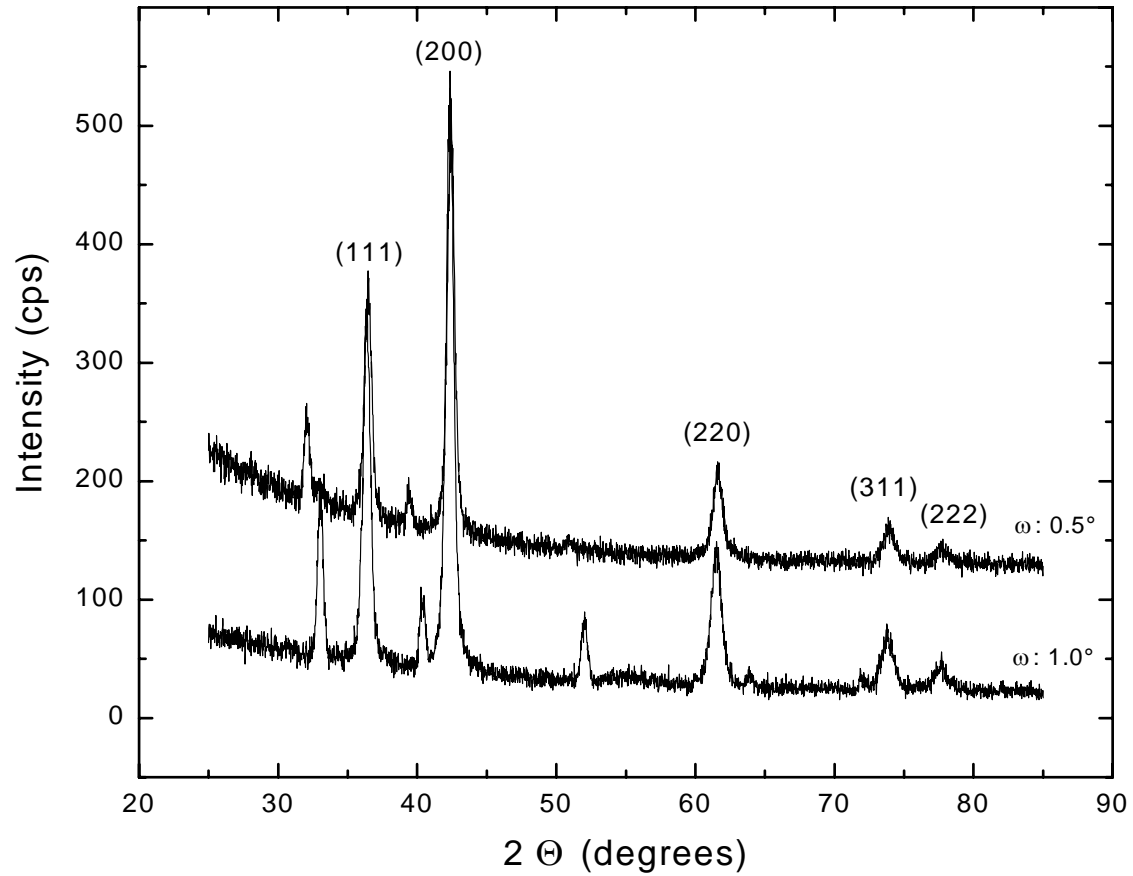
Simulation of the reflectivity of a 30 nm Al-layer on Si with varied roughnesses σ_1 (air-Al) and σ_2 (Al-Si) : curve a: $\sigma_1, \sigma_2 = 0$ nm; curve b: $\sigma_1 = 2$ nm, $\sigma_2 = 0$ nm; curve c: $\sigma_1 = 0$ nm, $\sigma_2 = 2$ nm; curve d: $\sigma_1, \sigma_2 = 2$ nm.

Beispiele

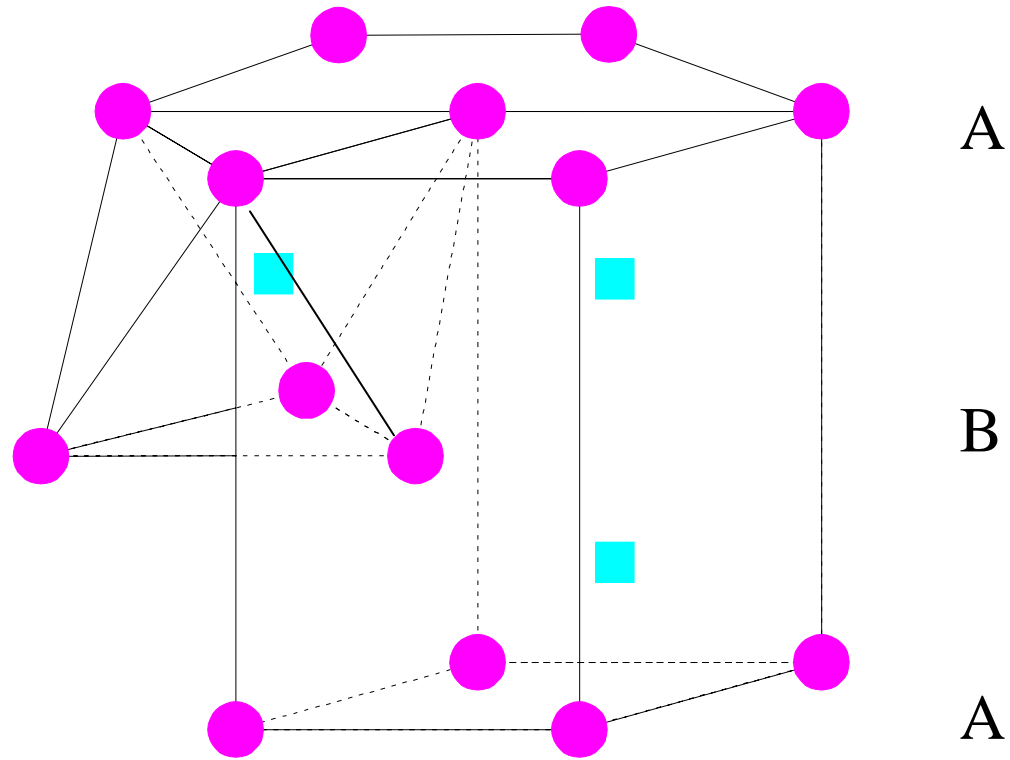
3.1. Phasenanalyse: Ti- TiN_x



Film composition determined by XPS (▲) and interplanar spacings of (002) α-Ti (*) and (111) δ-TiN_x planes (●) versus N₂ gas flow



Grazing incidence diffractometry patterns at different incident angles of 50 nm thick TiN_x films deposited at 60 sccm N₂ flow

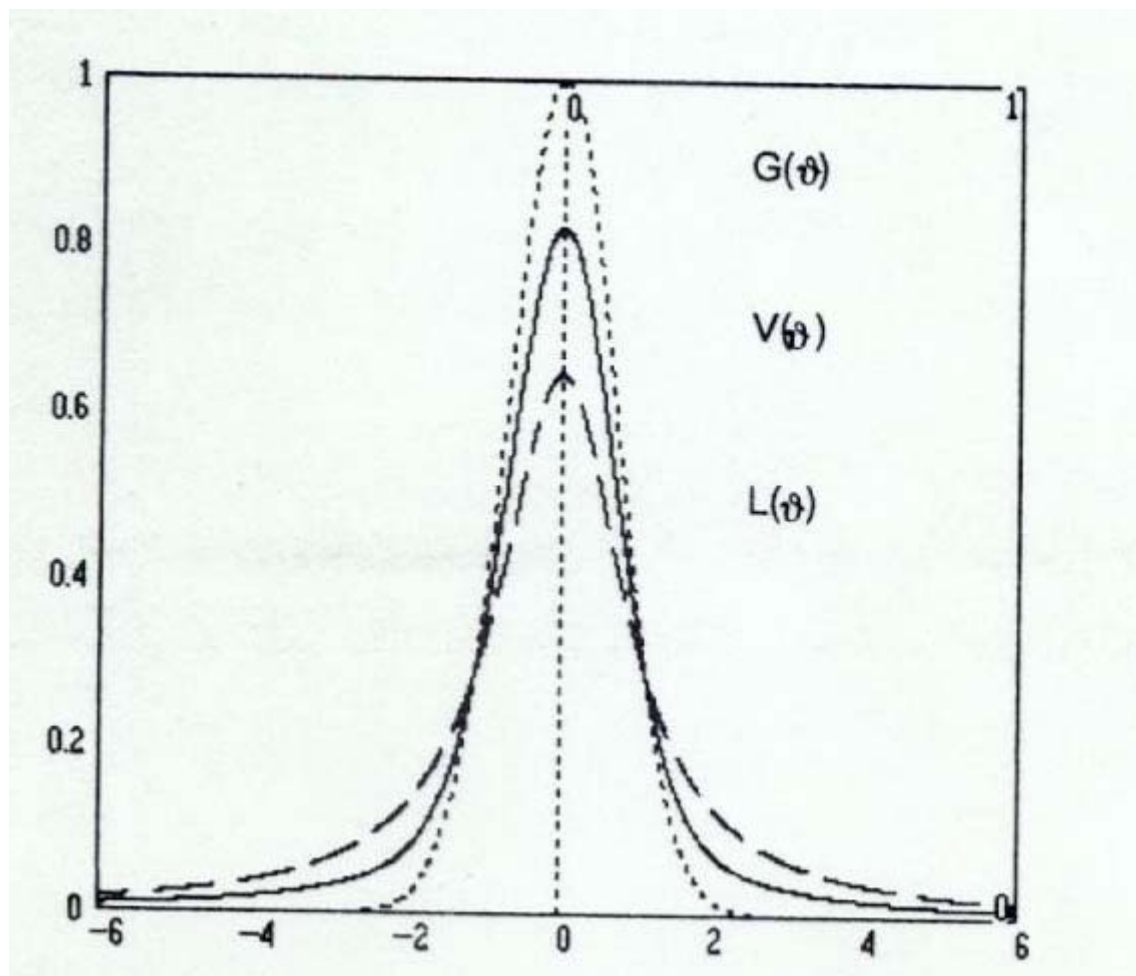


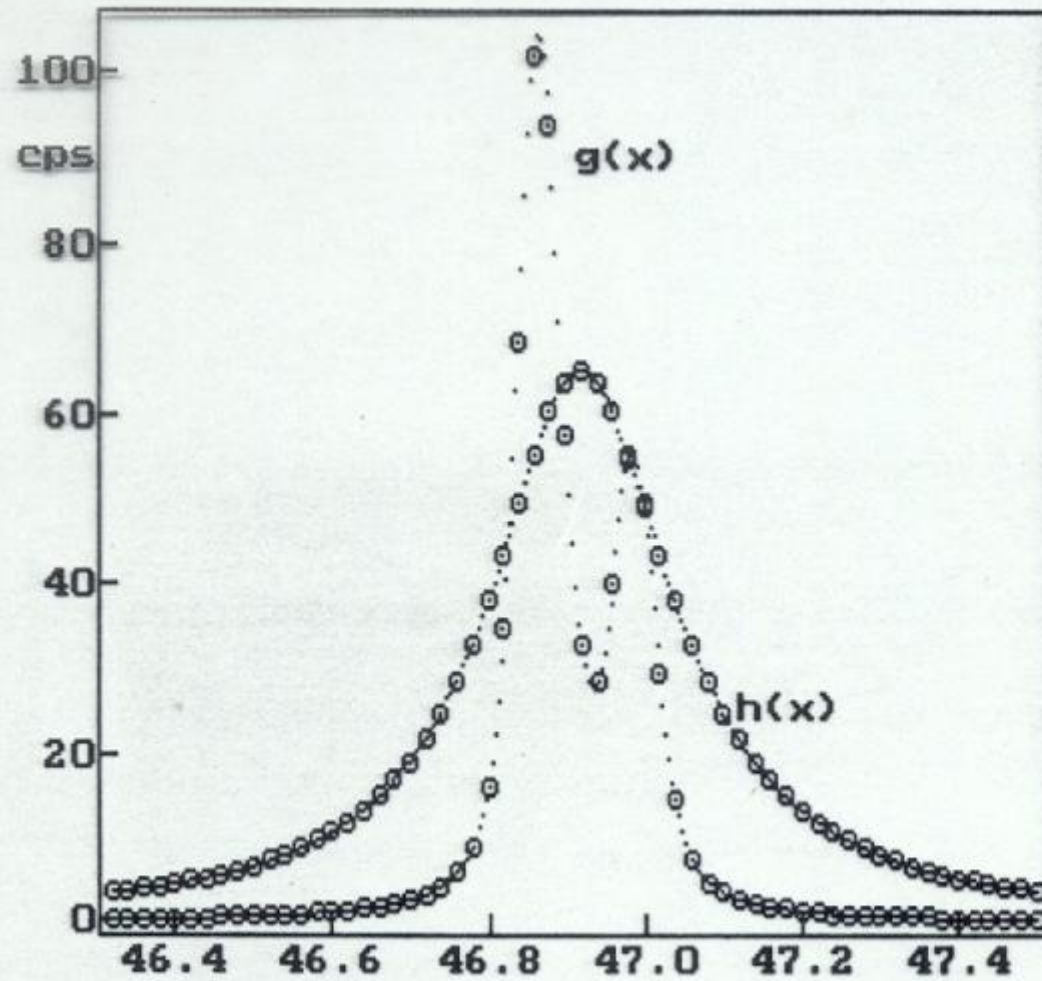
■ in $2/3 \ 1/3 \ 1/4, 2/3 \ 1/3 \ 3/4$

Crystal structure of α -Ti (hcp)

3.2. Defektstrukturanalyse

Ti- TiN_x





X-ray profile analysis

$$h(x) = \int f(y) * g(x - y) dy$$

$$F(L) = \frac{H(L)}{G(L)} \quad \text{STOKES method}$$

F(L), H(L) G(L) are the Fourier Transforms
of f(x), h(x) and g(x)
normalized to $F(0) = H(0) = G(0) = 1$

$$F(L) = A_p(L) * A_s(L) * A_d(L)$$

$$F(L) = \exp(-L/T) * \exp(-K \langle \varepsilon^2 \rangle L^2) * \exp(-B \ln(L_0/L) L^2)$$

and

$$-\ln F(L) = L/T + \langle K \langle \varepsilon^2 \rangle + B \ln(L_0/L) \rangle L^2$$

$$L = n * d(hkl)$$

domain of definition of experimental line profile

$$T = T(hkl)$$

effective particle size

$$B = B(hkl)$$

mean total dislocation density

$$L_0$$

length proportional to the core radius r_0 of the strain field of dislocation

$$\langle \varepsilon^2 \rangle = \langle \varepsilon^2(hkl) \rangle$$

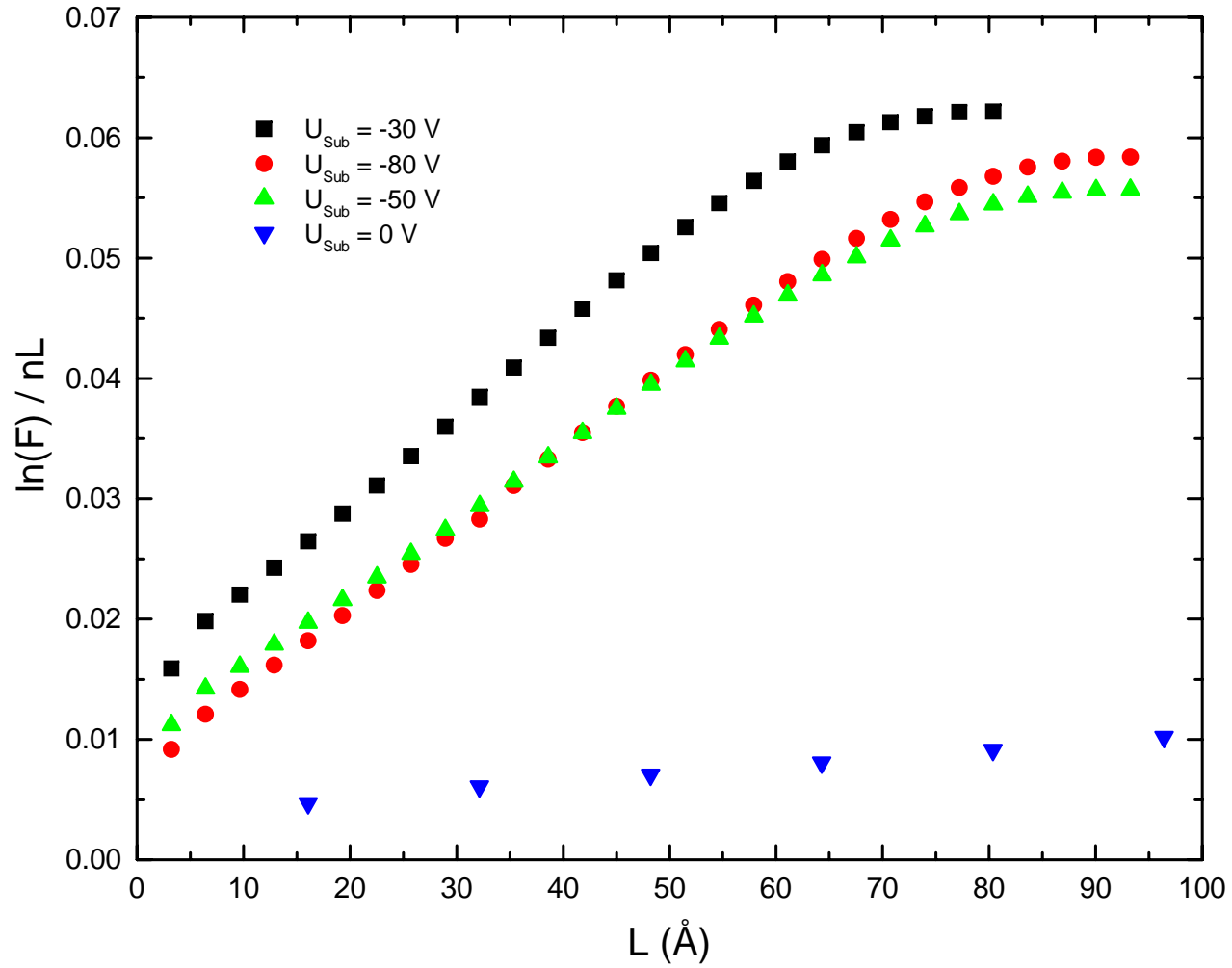
mean square microstrain due to internal stress

WARREN-AVERBACH-plot

$$-\ln F(L) / L = 1/T + K \langle \varepsilon^2(L) \rangle L$$

KRIVOGLAZ-WILKENS-plot

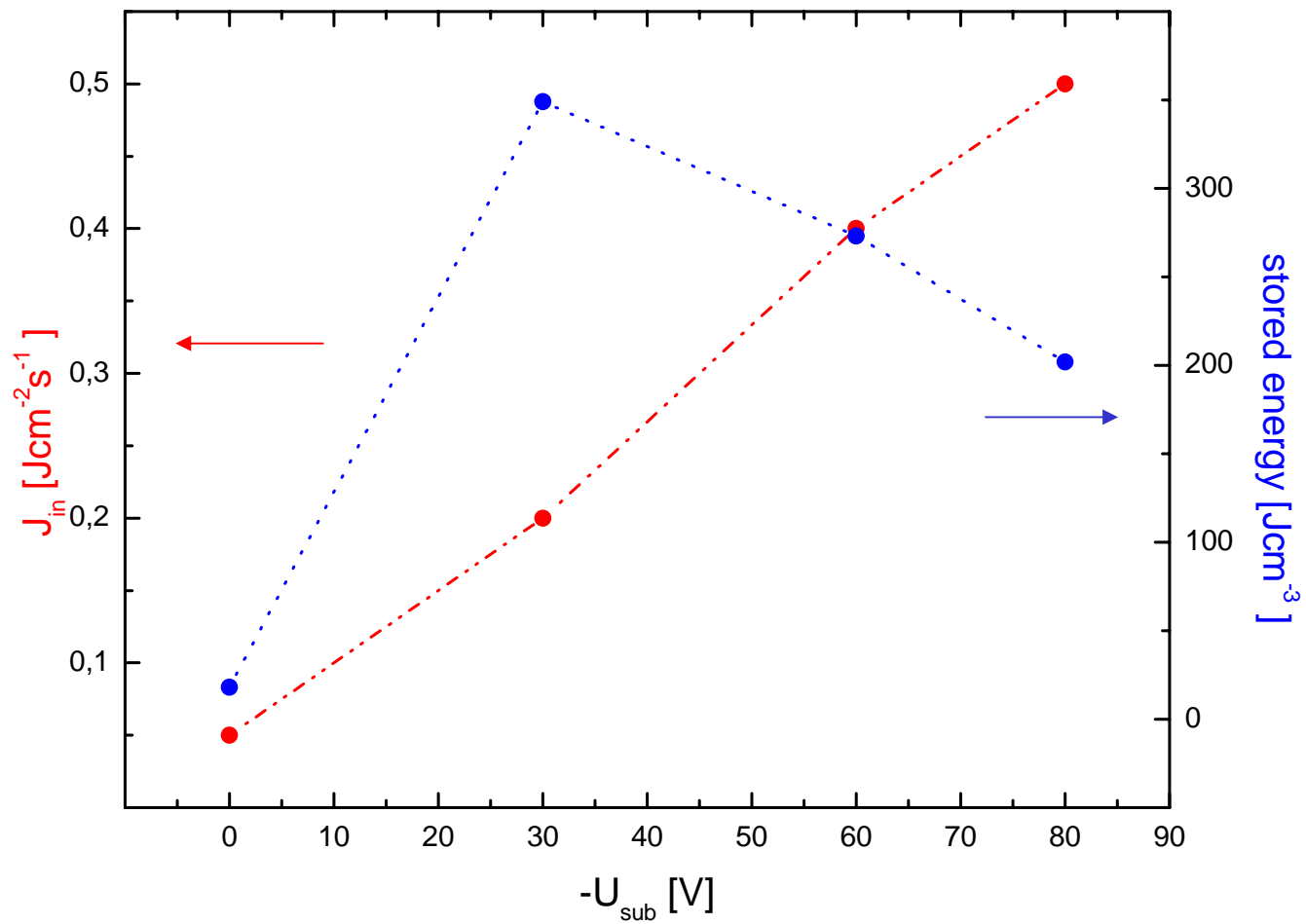
$$-\ln F(L) / L^2 = 1/TL + (K \langle \varepsilon^2 \rangle + B \ln L_0) - B \ln L$$



Warren-Averbach plot of TiN_x films deposited at constant N_2 gas flow and various substrate voltages

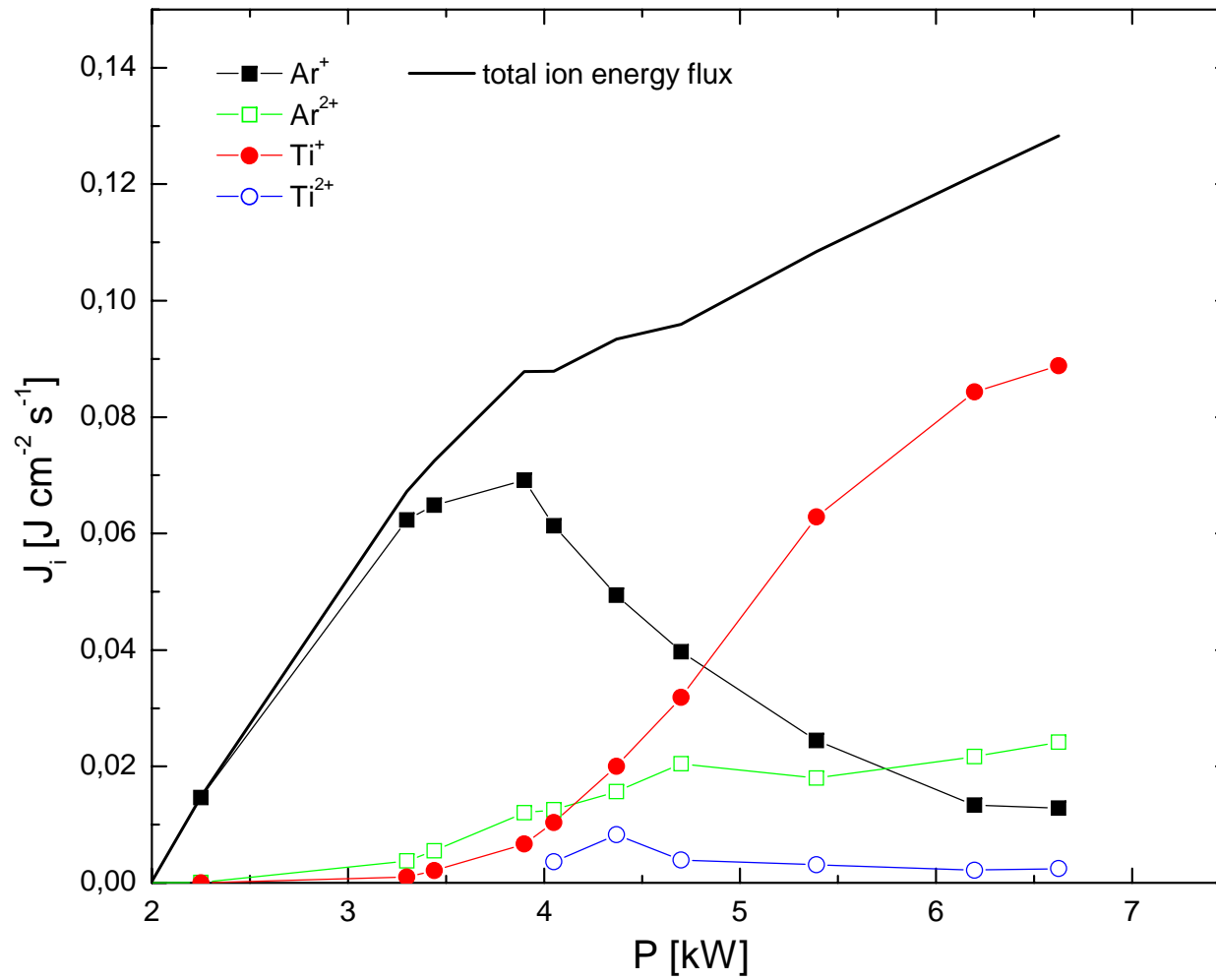
U_{sub}/V	0	-30	-50	-80
N/Ti	0.57	0.62	0.68	0.85
$d_{III}A^\circ$	2.419	2.443	2.447	2.448
T/A°	253	67	99	130
$\langle \varepsilon^2 \rangle^{1/2} * 10^3$	4.45	14.9	13.6	14.2
$p_v * 10^{11}/cm^{-2}$	2.7	36	28	24
$C_i/\%$	reference	1.9	1.67	0.39
$E(st) J/cm^3$	23	339	273	202

Physical parameters of TiN_x deposited at various substrate voltages

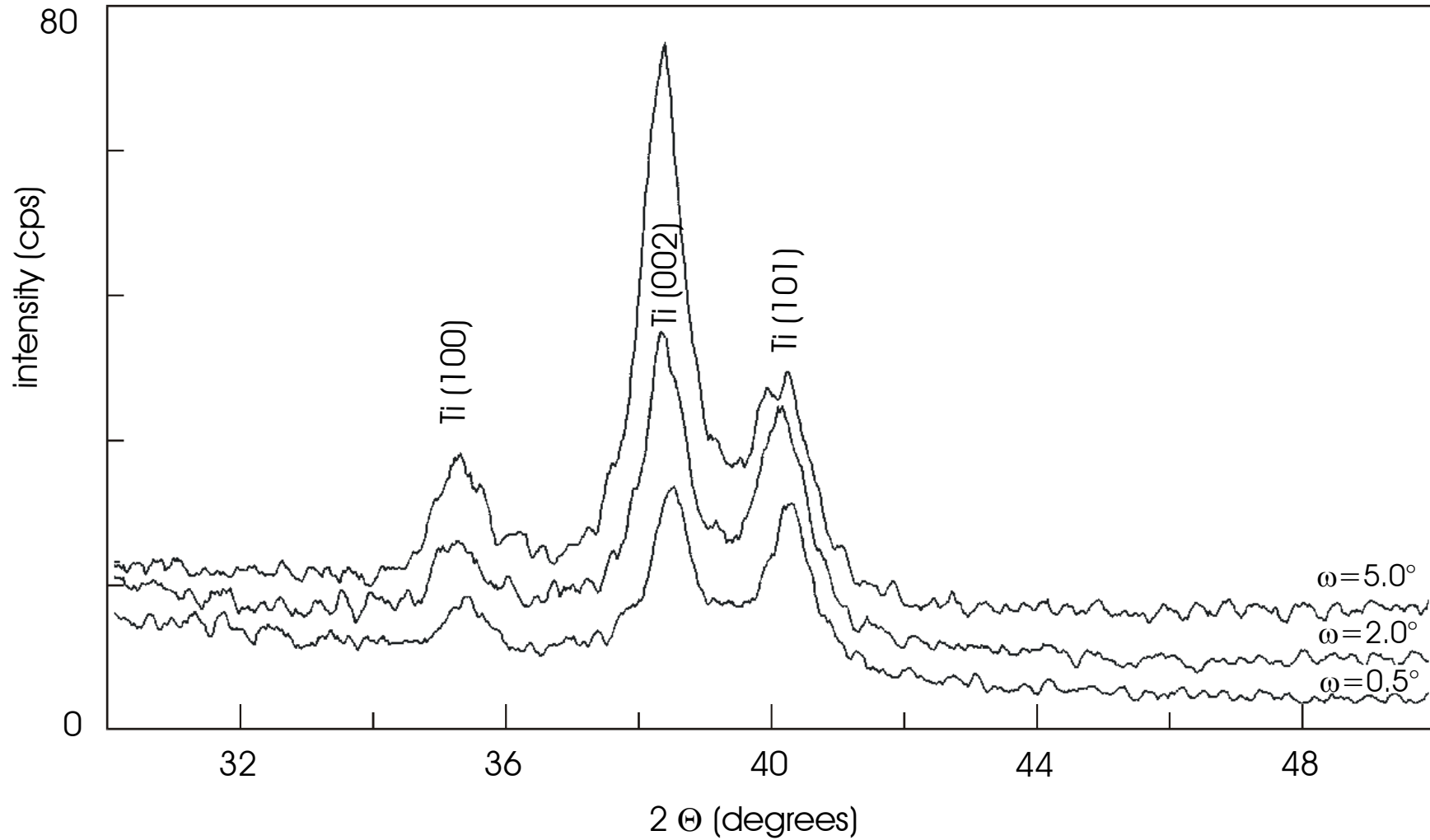


Energy flux to the surface and stored energy in the TiN-films vs substrate voltage

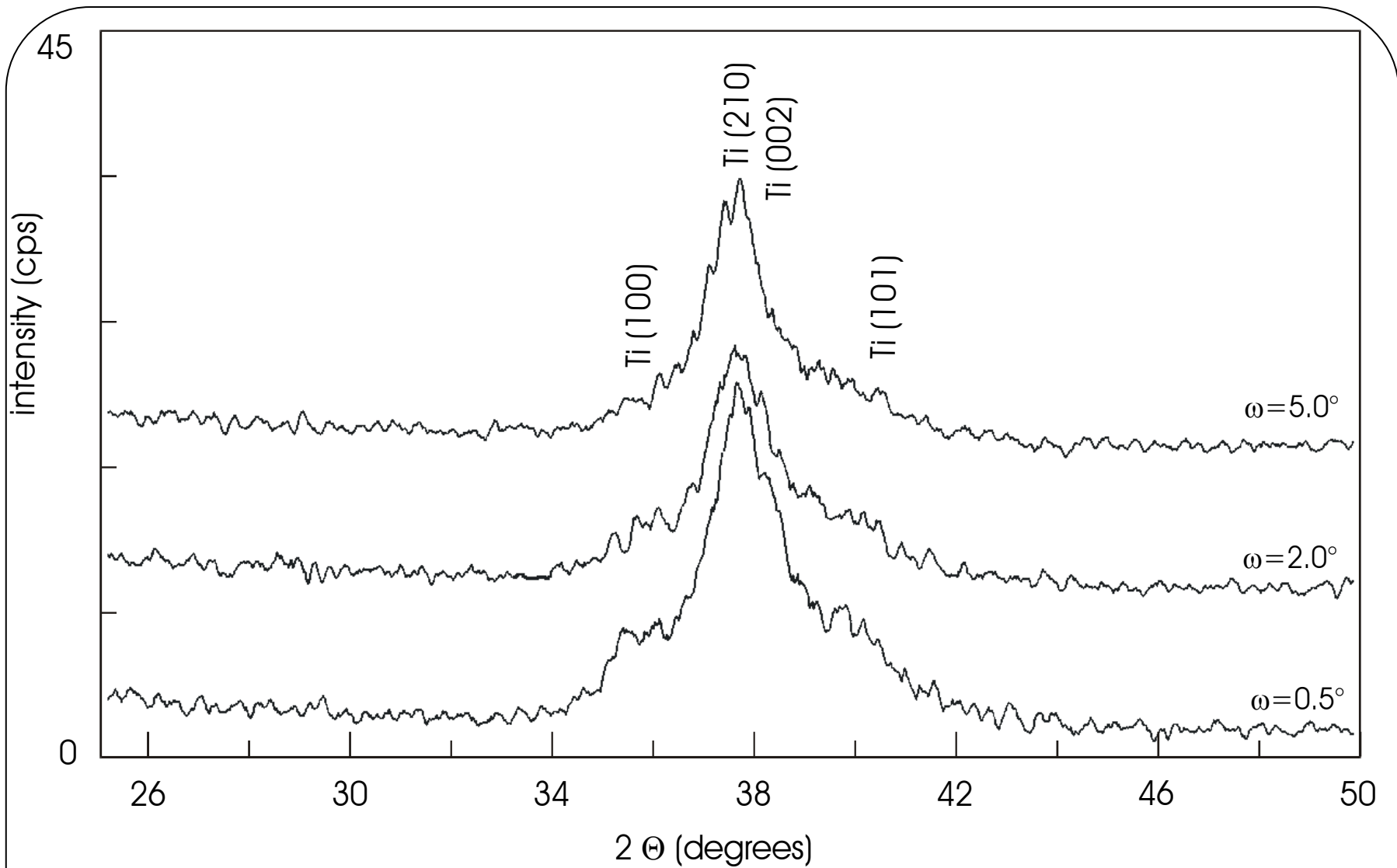
3.3. Berechnung von Strukturgradienten : Ti- TiSi



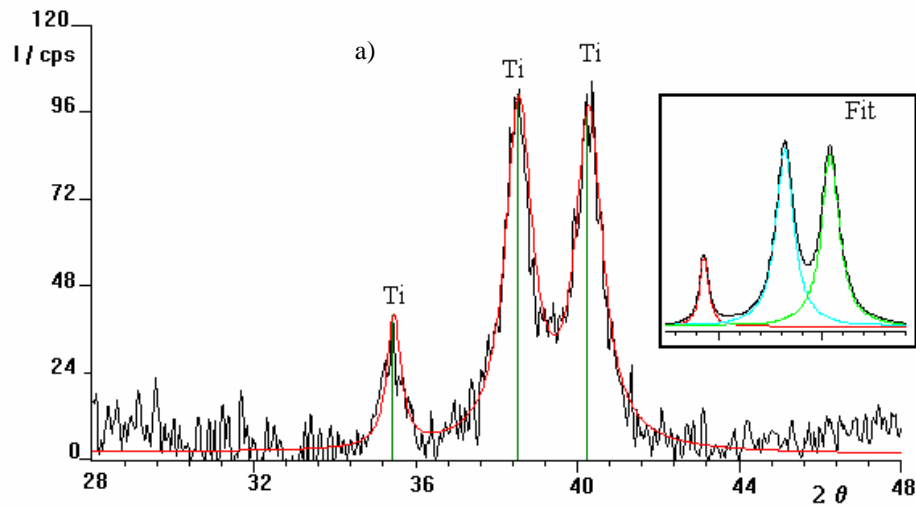
Ion-energy-flux to the substrate vs plasma power



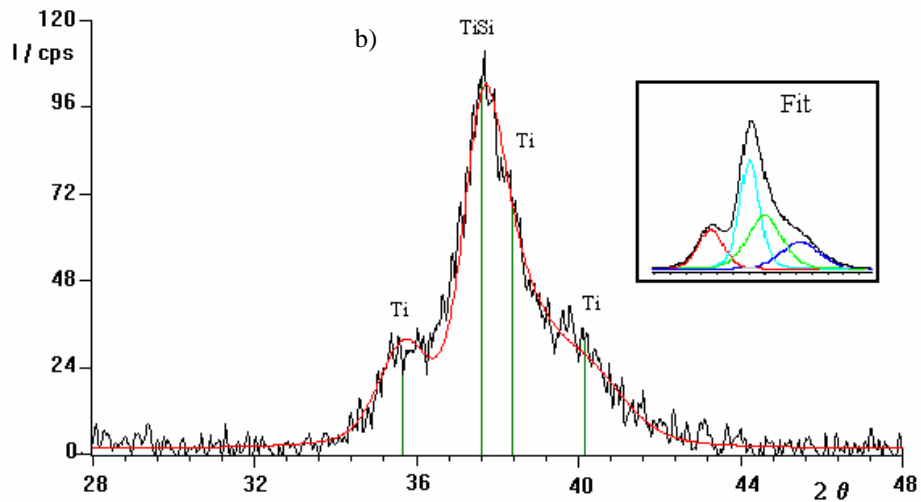
GIXD pattern of Ti-films deposited at high discharge power (sample 1) at different incident angles ω .



GIXD pattern of Ti-films deposited at low discharge power (sample 2) at different incident angles ω .



Fit procedures for
(a) sample 1 high discharge power
(b) sample 2 low discharge power



The X-ray parameters measured represent **absorption weighted effective parameters, different from the true values**. In general, for absorption weighted mean y_{eff} of X-ray parameters holds:

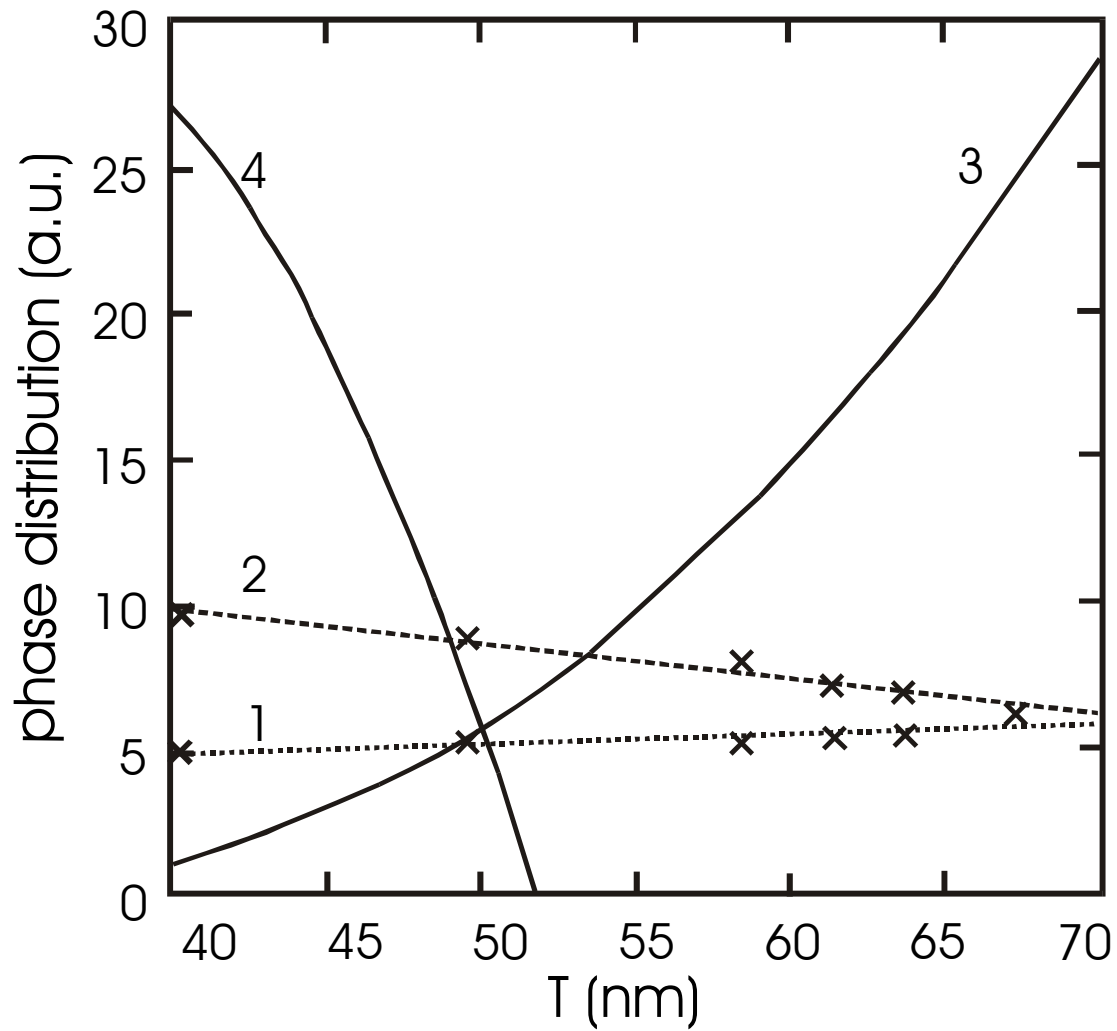
$$y_{eff}(T) = \frac{\int_0^{x_0} y(x) \cdot \exp\left(\frac{-x}{T}\right) dx}{\int_0^{x_0} \exp\left(\frac{-x}{T}\right) dx}$$

The aim of a layer analysis is the calculation of true values $y(x)$ from effective parameters y_{eff}

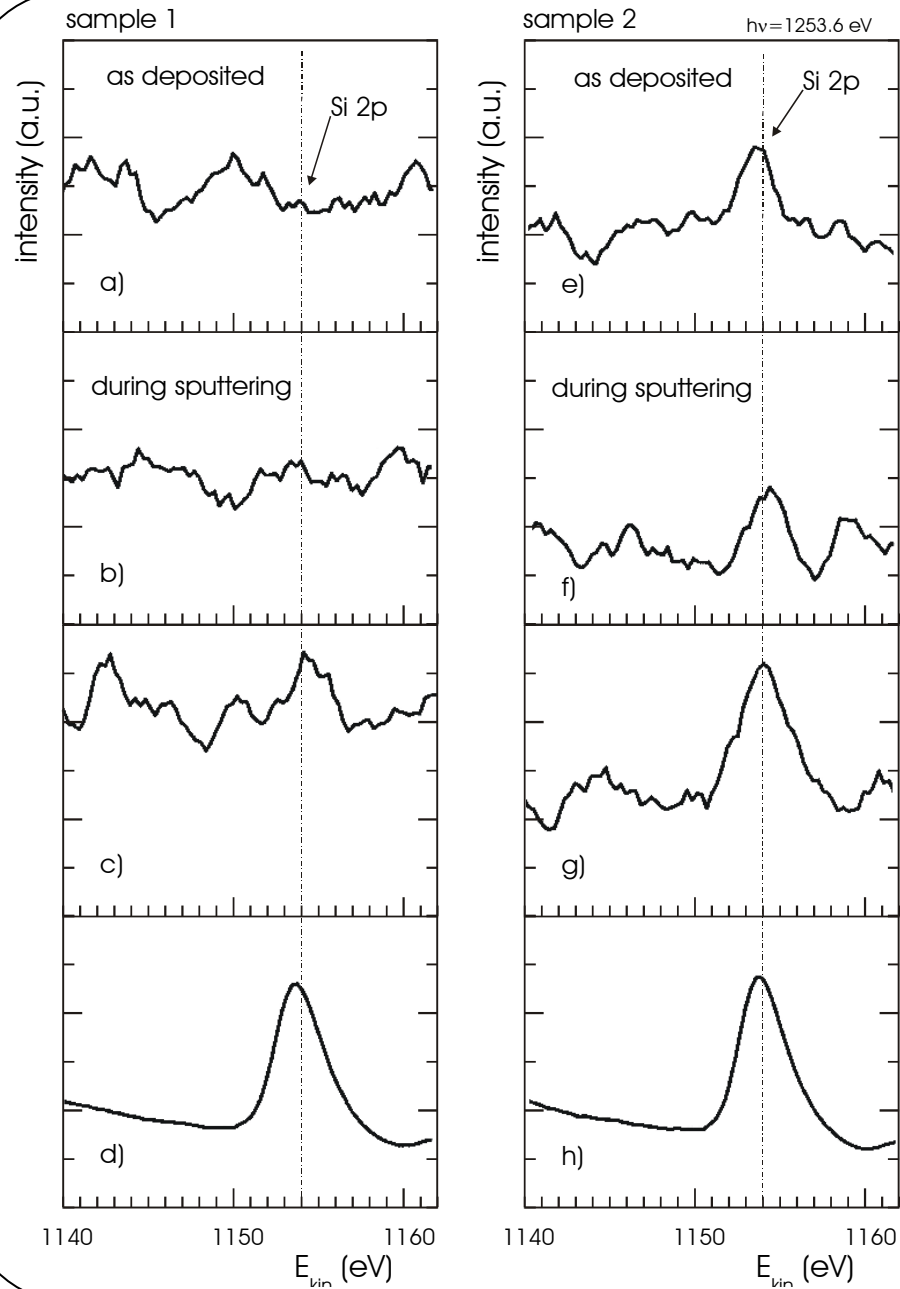
The $y_{eff}(T)$ are measured by varying the incidence angle ω in the GIXD.

Common solutions are possible if the $y(x)$ are approximated by Fourier series or by polynomials as:

$$y(x) = \sum_m a_m \cdot x^m$$



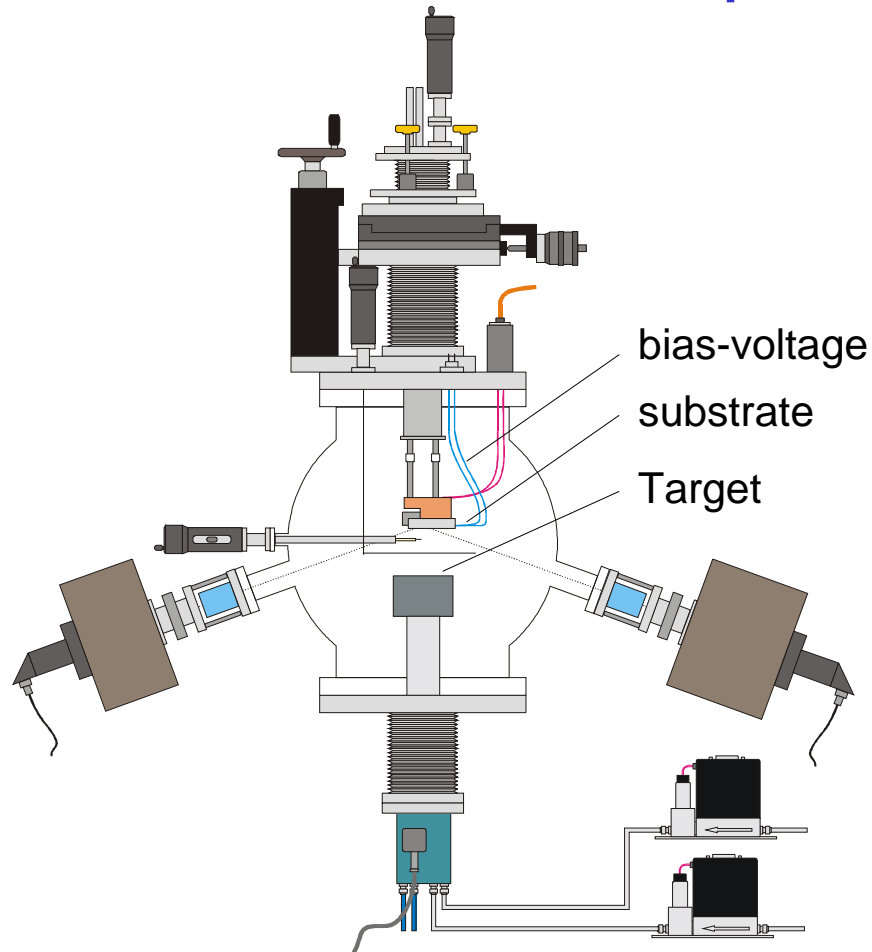
Effective integral intensities of the TiSi (210) peak (curve 1) and the α -Ti (100) peak (curve 2) and the calculated distribution of the crystalline phases TiSi (curve 3) and Ti (curve 4).



XPS of Ti on Si deposited at
 (a) – (d) high discharge power and
 (e) – (h) low discharge power

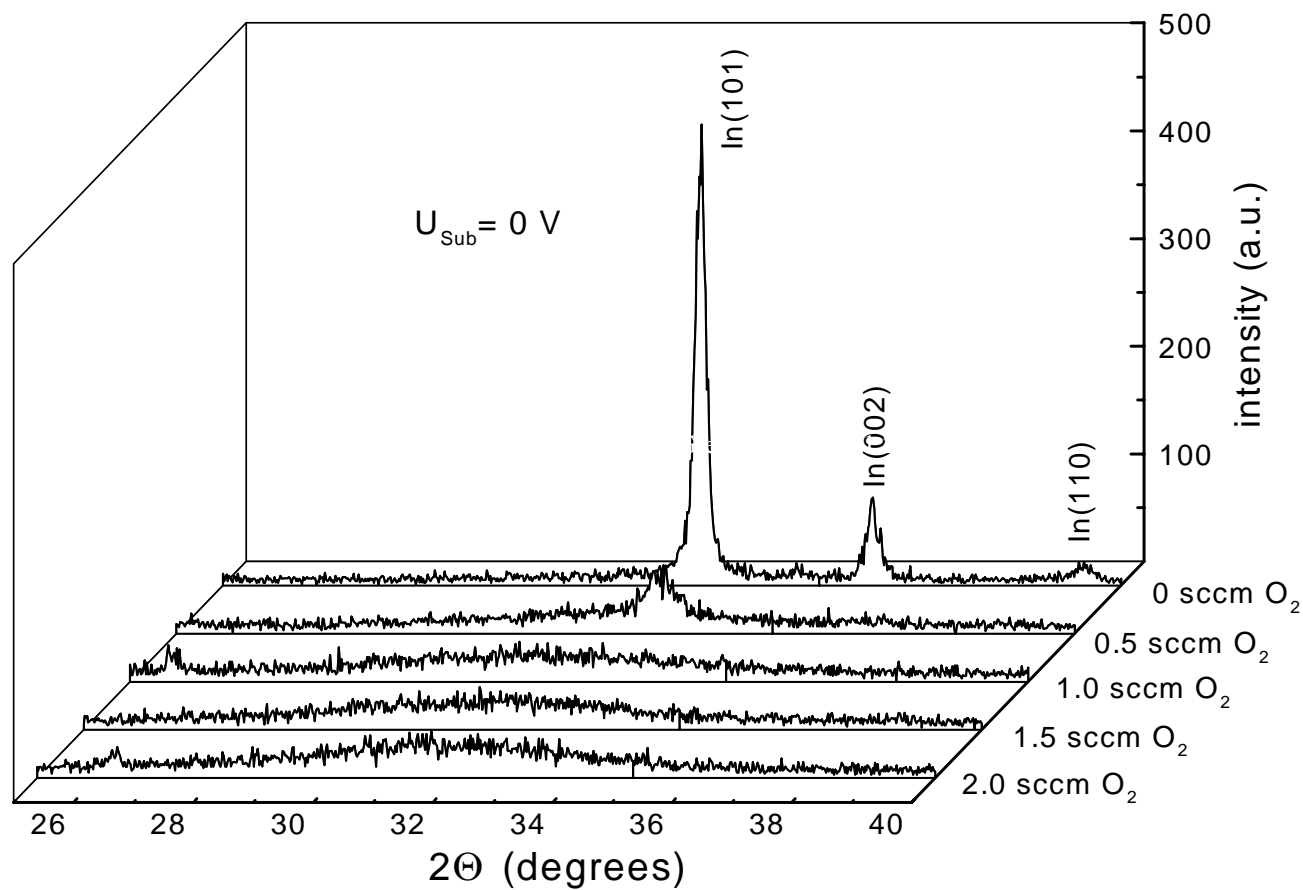
3.4. Studium kinetischer Prozesse ITO

Experimental

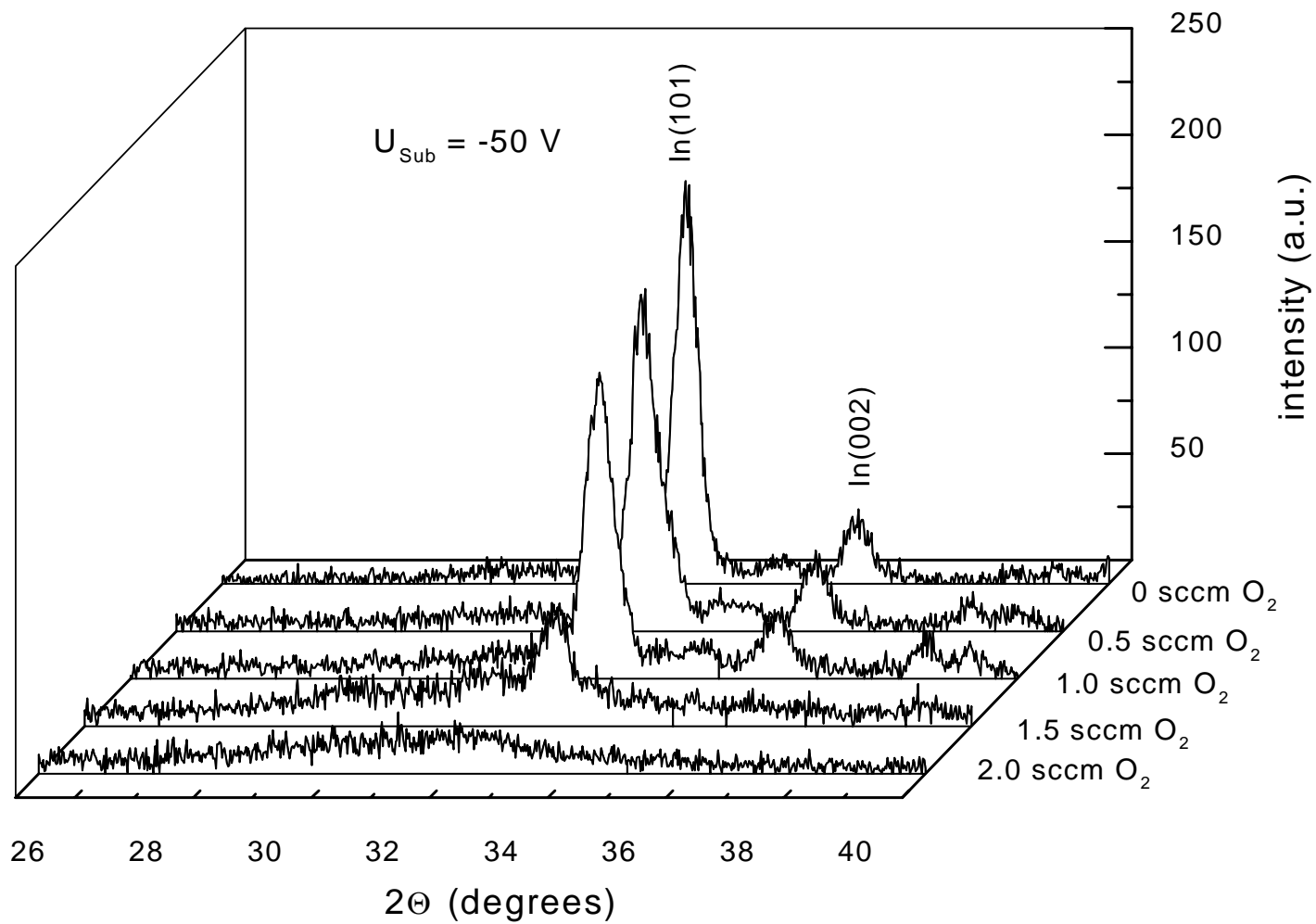


film deposition by dc magnetron sputtering at different bias voltages and reactive gas flows

sputtering-parameter	30 W, 350 V, 85 mA
target	5" In/Sn (90/10)
substrate	Si(100)-wafer
distance target-substrate	60 mm
total pressure	$5,6 \cdot 10^{-3}$ mbar
sputtering gas	15 sccm Argon
reactive gas	0 ... 2 sccm Oxygen
substrate voltage	0, - 50, -100 V
film thickness	50 nm



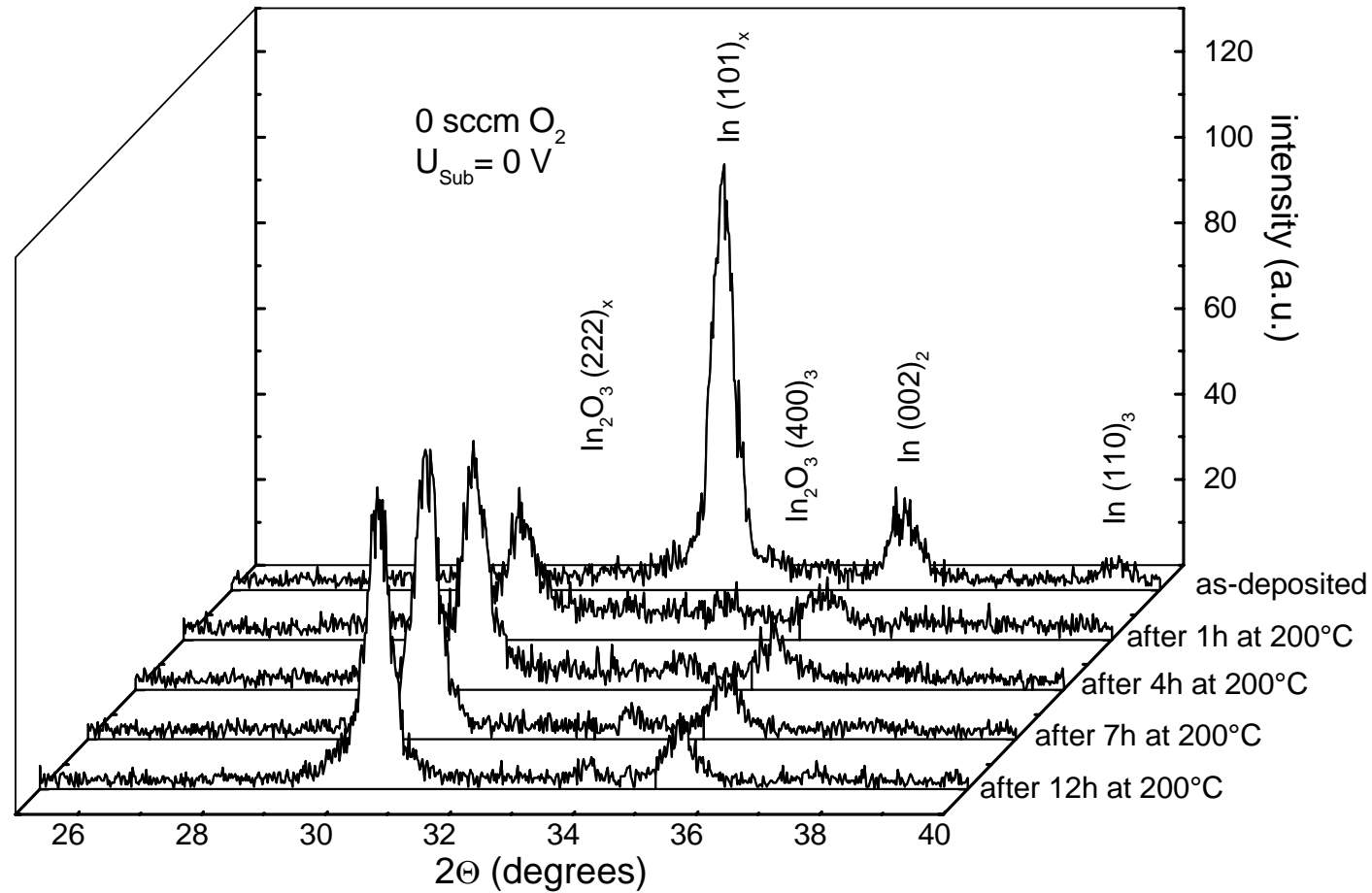
Diffraction patterns of ITO-films deposited at different oxygen flows, $U_{\text{sub}} = 0 \text{ V}$



Diffraction patterns of films deposited at different oxygen flows, $U_{\text{sub}} = -50 \text{ V}$

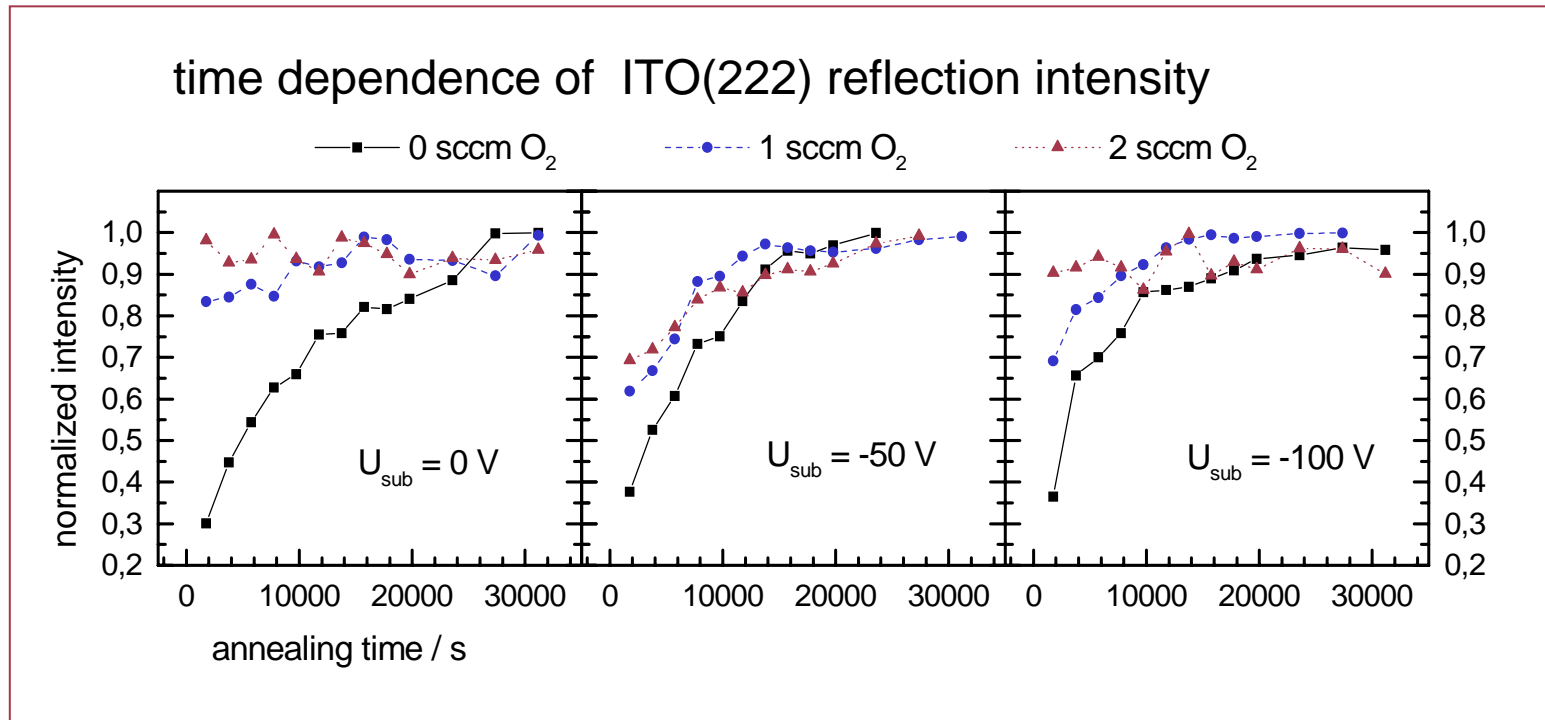
A: Diffusion

Annealing process - in situ high temperature diffractometry



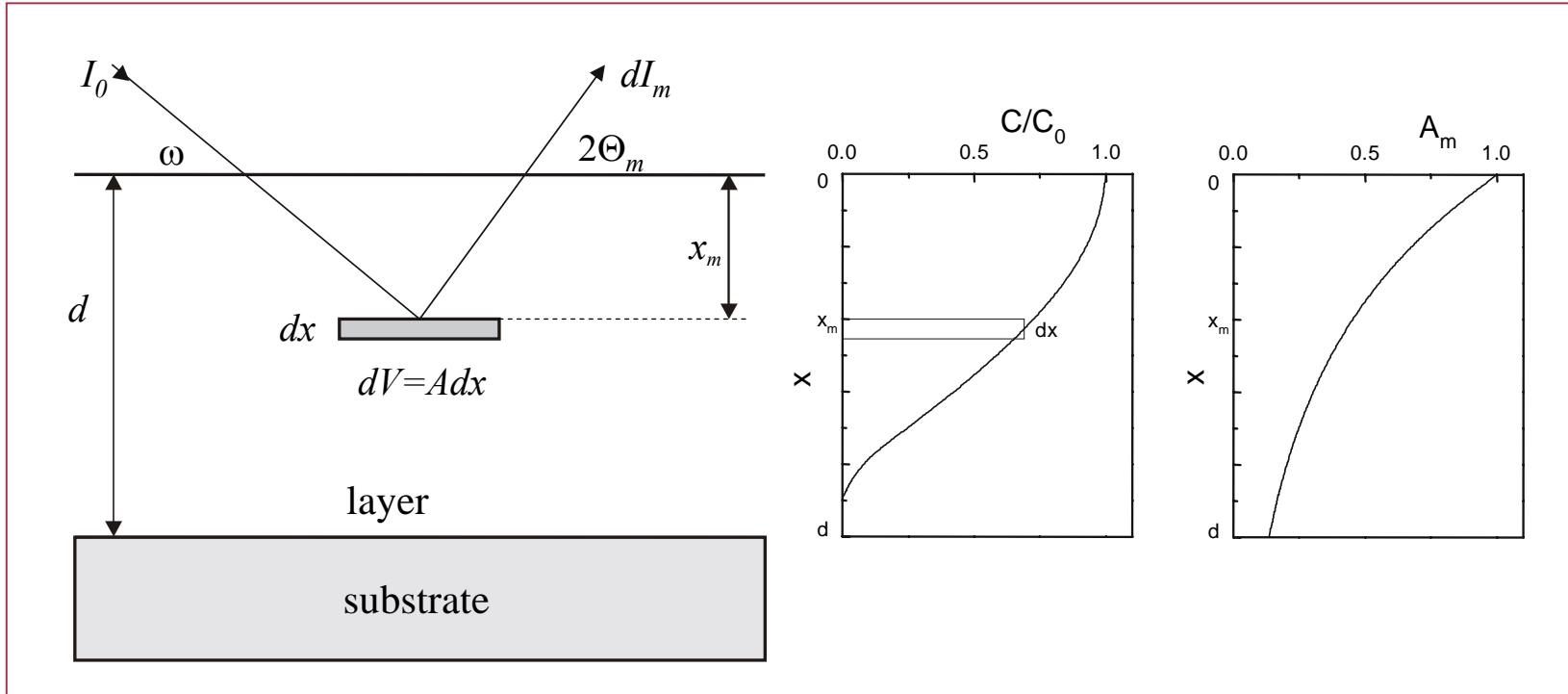
Phase transformation of metallic In/Sn into crystalline ITO at 200°C

High temperature grazing incidence x-ray diffractometry



- ITO formation depends on deposition conditions
- slow conversion of metallic In/Sn, intensity increases with sqrt of time, that means a diffusion limited process takes place
- fast crystallization of amorphous ITO

in-situ determination of diffusion coefficients from time dependence of x-ray reflections



$$I_m(t) = B_m K_0 I_0 A \int_0^d C(x,t)/C_0 A_m dx$$

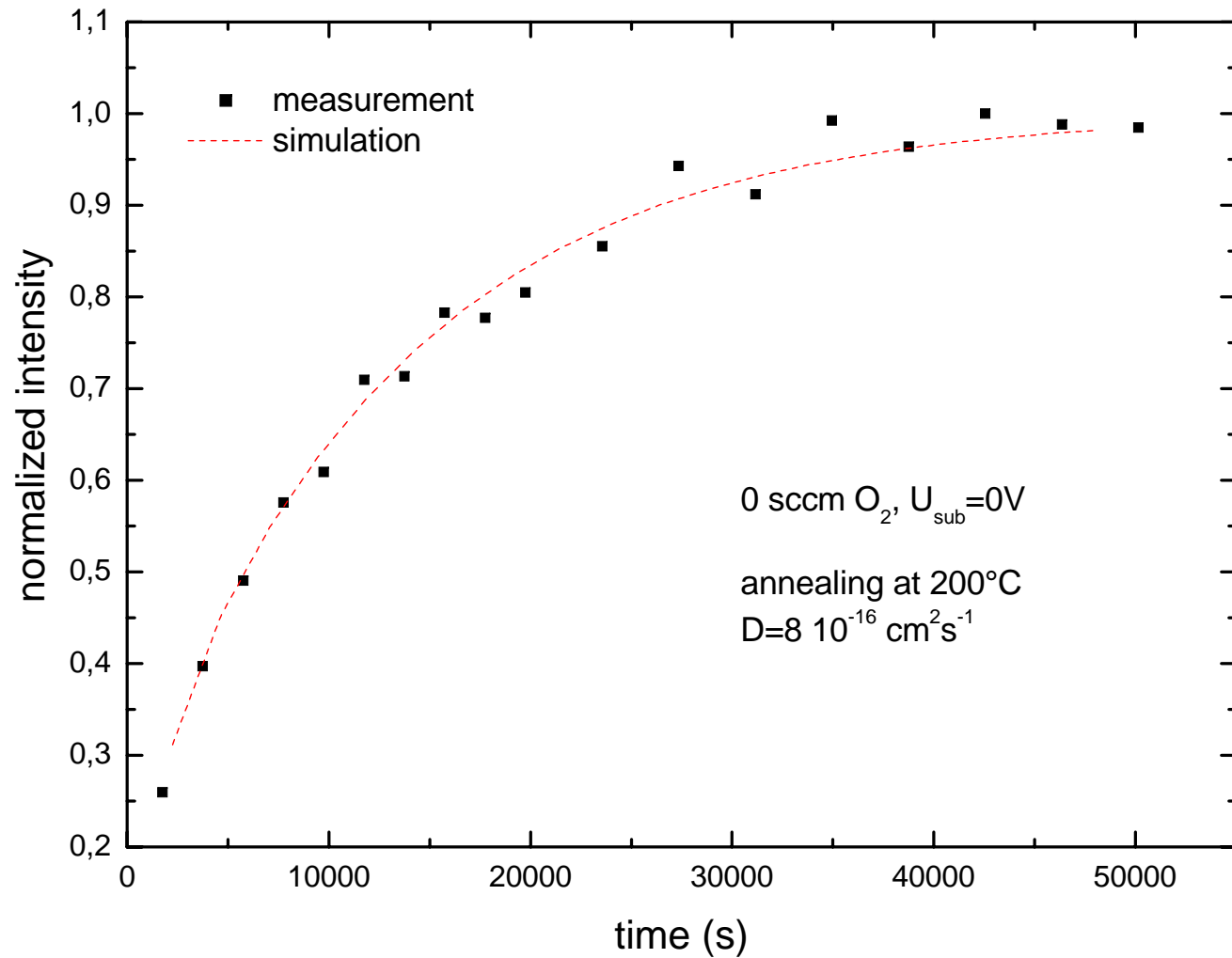
$$A_m = e^{-\bar{\mu}(x,t) z_m x_m}$$

$$\bar{\mu} = (\mu_m - \mu_n) f + (\mu_m - \mu_n)(1-f) \frac{1}{x_m} \int_0^{x_m} \frac{C^1}{C_0^1} dx + \mu_n$$

$$\frac{\partial C(x,t)}{\partial t} = D \frac{\partial^2 C(x,t)}{\partial x^2}$$

**Fick's
Second Law**

$$\frac{C^1(x,t)}{C_0^1} = 1 - \frac{4}{\pi} \sum_{n=1}^{\infty} \frac{(-1)^{n-1}}{2n-1} \cos\left(\frac{2n-1}{2} \pi \frac{d-x}{d}\right) e^{-\left(\frac{2n-1}{2} \pi\right)^2 \frac{Dt}{d^2}}$$



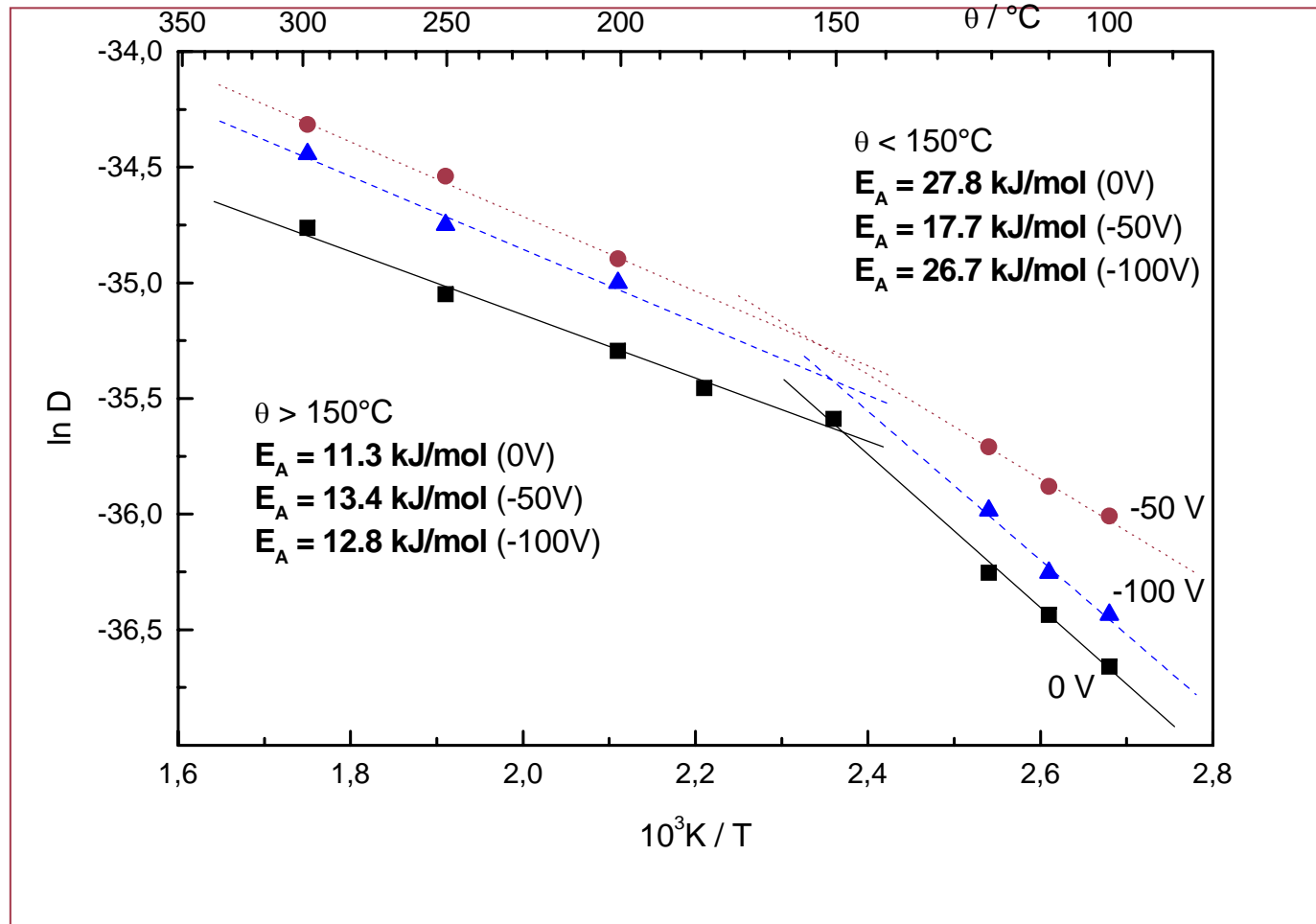
The measured normalized X-ray integral intensities of ITO (222) reflection and the calculated intensity values (dashed line) versus time of a film deposited at 0 sccm O₂ and 0 V bias voltage

O_2 -flow [sccm]	$U_{substr.}$ [V]	D [$cm^2 s^{-1}$]	f (amorphous ITO)
0	0	$6.0 \cdot 10^{-16}$	0
0.5		$5.5 \cdot 10^{-16}$	0.5
1.0		$6.0 \cdot 10^{-16}$	0.75
1.5		-	1
2.0		-	1
0	-50	$13.0 \cdot 10^{-16}$	0
0.5		$16.5 \cdot 10^{-16}$	0
1.0		$14.1 \cdot 10^{-16}$	0.3
1.5		$14.9 \cdot 10^{-16}$	0.5
2.0		$15.6 \cdot 10^{-16}$	0.7
0	-100	$9.4 \cdot 10^{-16}$	0
0.5		$9.1 \cdot 10^{-16}$	0
1.0		$9.6 \cdot 10^{-16}$	0.5
1.5		$9.6 \cdot 10^{-16}$	0.65
2.0		$9.6 \cdot 10^{-16}$	0.8

effective diffusion coefficients

- independent of oxygen flow
- no InO_x -phases, coexistence of crystalline In/Sn domains and amorphous ITO
- depend on substrate voltage

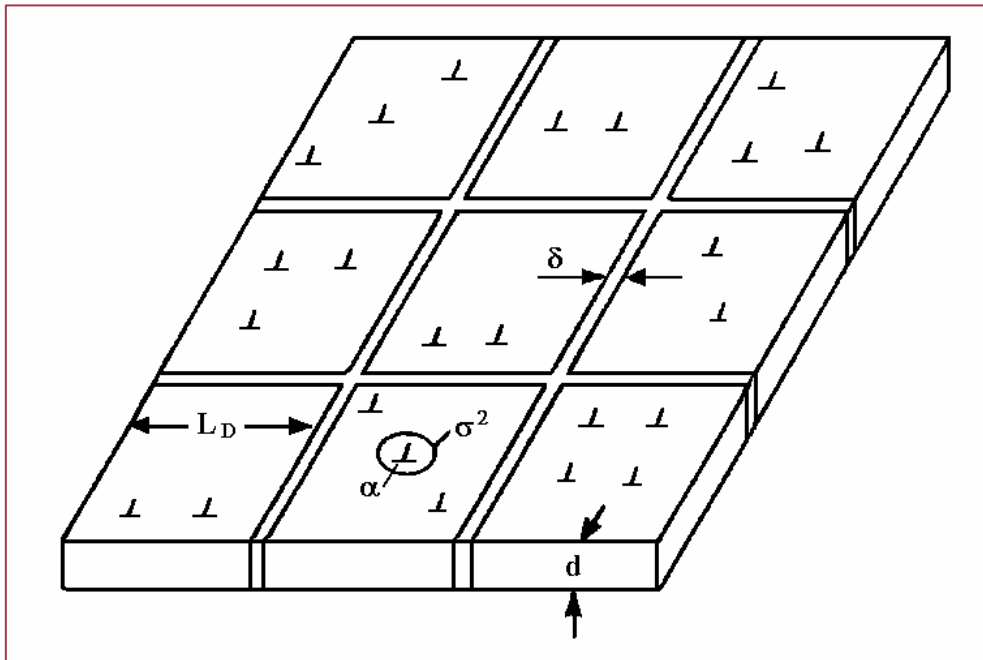
Activation energy for oxygen diffusion



- Arrhenius plot for the diffusion process, two different activation energies were found, influence of film microstructure only for $T < 150^\circ C$

Diffusion within a polycrystalline film

$$D_{eff} = D_L + \frac{\delta}{L_D} D_{GB} + \alpha \sigma^2 D_{Disl} = D_L \left(1 + \frac{\delta}{L_D} \frac{D_{GB}}{D_L} + \alpha \sigma^2 \frac{D_{Disl}}{D_L} \right)$$



- separation of the contributions of grain boundary (D_{GB}), dislocation (D_{disl}) and lattice (D_L) diffusion

- grain size determines the effective diffusion coefficient

- **main part** of the mass transport occurs along the **grain boundaries**

$$\frac{D_{GB}}{D_L} = \frac{\exp(-E_{A(GB)} / RT)}{\exp(-E_{A(L)} / RT)} \quad \frac{D_D}{D_L} = \frac{\exp(-E_{A(D)} / RT)}{\exp(-E_{A(L)} / RT)}$$

$$D_{eff} (100^\circ C) = D_L (1 + 372.3 + 0.4)$$

0V

$$D_{eff} (100^\circ C) = D_L (1 + 640.8 + 0.6)$$

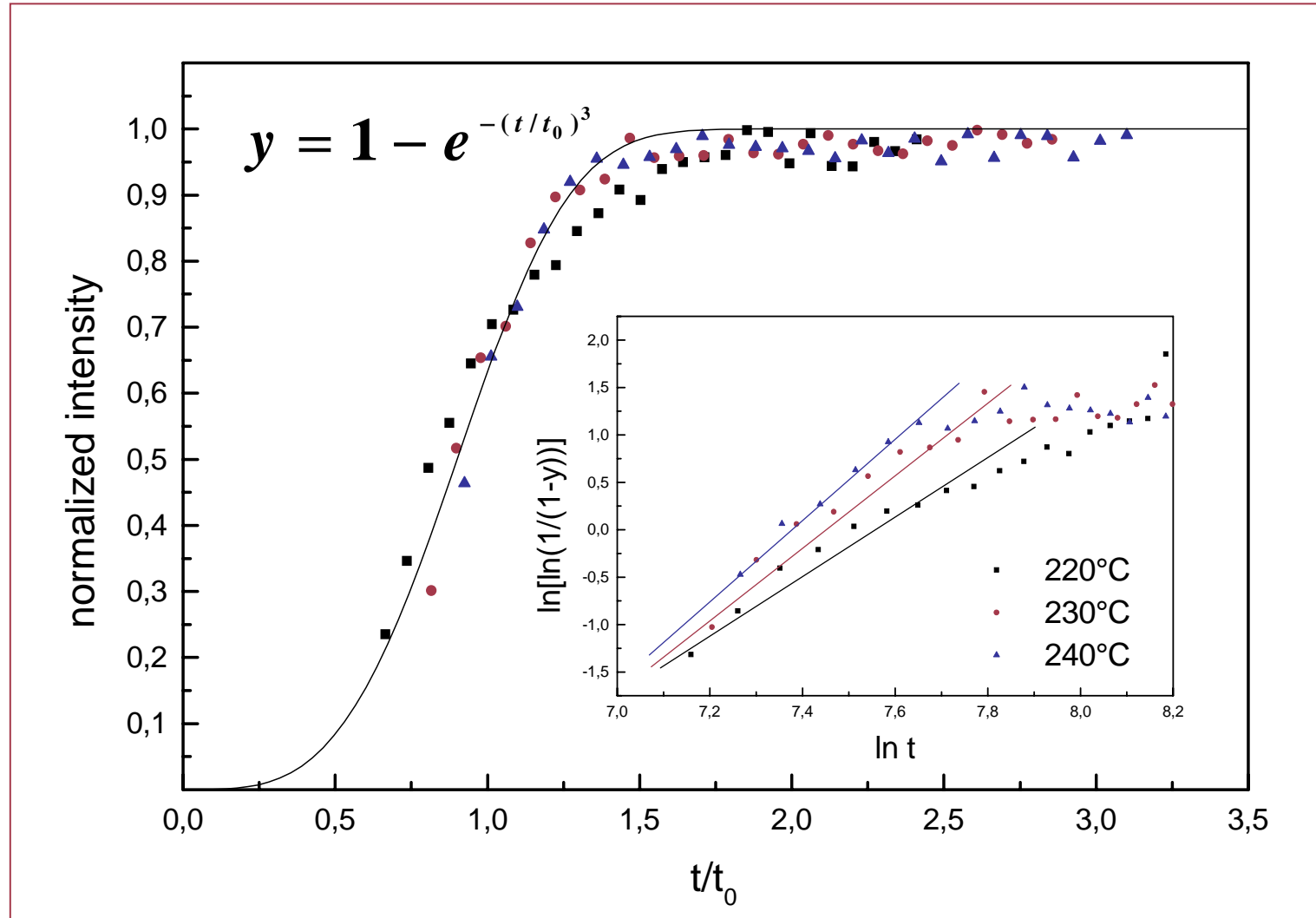
-50V

$$D_{eff} (100^\circ C) = D_L (1 + 388.1 + 0.5)$$

-100V

B: Kristallwachstum

Crystallization process, Johnson-Mehl-Avramy plot



Johnson-Mehl-Avrami theory

$$y = 1 - e^{-(t/t_0)^n}$$

y normalized intensity
t annealing time
n reaction order
1/t₀ rate constant

<i>T / °C</i>	<i>1/t₀</i>	<i>n</i>
220	4.5 · 10 ⁻⁴ s ⁻¹	2.4
230	7.1 · 10 ⁻⁴ s ⁻¹	2.8
240	8.9 · 10 ⁻⁴ s ⁻¹	3.0

- quantitative description of crystallization process using the integral intensity of x-ray reflection
- interpretation of data using the Johnson-Mehl-Avrami theory
- exponent n between 2.4 and 3.0, means **two dimensional crystallite growth** parallel to the surface
- activation energy for crystallization from amorphous ITO: E_A = 74 kJ mol⁻¹

3.5. Untersuchung von Clustern

Ag Cluster

Rechnungen zu Clustern und experimentelle
Überprüfung

$$d\mu_i = \frac{dg}{dn_i} = -SdT + Vdp + RTd \ln a_i + \sigma dO$$

für reine Stoffe

$$dG_s = V_s dp - S_s dT + \sigma dO_s$$

$$dG_g = V_g dp - S_g dT$$

Gleichgewicht fest - gasförmig und konstante Temperatur

$$dg = dG_g - dG_s = 0 \quad (V_g - V_s)dp = \sigma dO$$

$$\frac{RT}{p} dp = \sigma dO = RTd \ln p \quad \text{für} \quad \frac{dm}{M} = dn \quad \text{Mole gilt:}$$

$$\frac{dm}{M} RTd \ln p = \sigma df$$

und

$$RT \ln \frac{p}{p_\infty} = \sigma \frac{df}{dn}$$

Für kleine würfelförmige Kristallite mit der Kantenlänge r gilt: $f = 6r^2$

$$df = 12rdr \quad \text{mit} \quad m = r^3 \cdot \rho \quad \text{und} \quad dm = 3r^2 \cdot \rho \cdot dr$$

$$\text{gilt:} \quad df = \frac{12r dm}{3r^2 \rho} = \frac{4dm}{r\rho}$$

$$dg = \sigma df = \frac{4\sigma dm}{r\rho} = \frac{dm}{M} RT \ln \frac{p}{p_\infty}$$

$$RT \ln \frac{p}{p_\infty} = \frac{4 \cdot \sigma \cdot M}{r \cdot \rho}$$

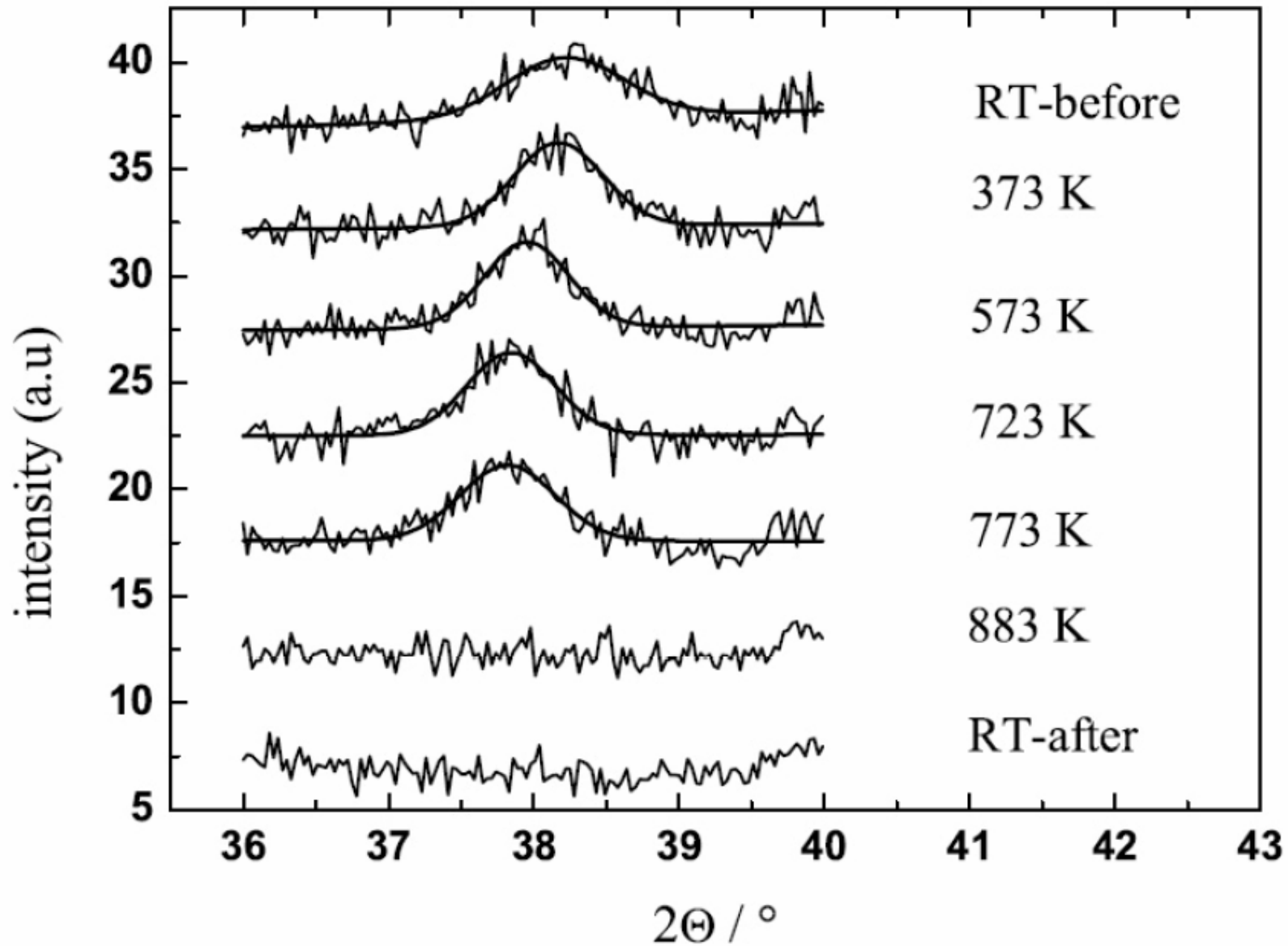
Clausius-Clapeyron Gleichung

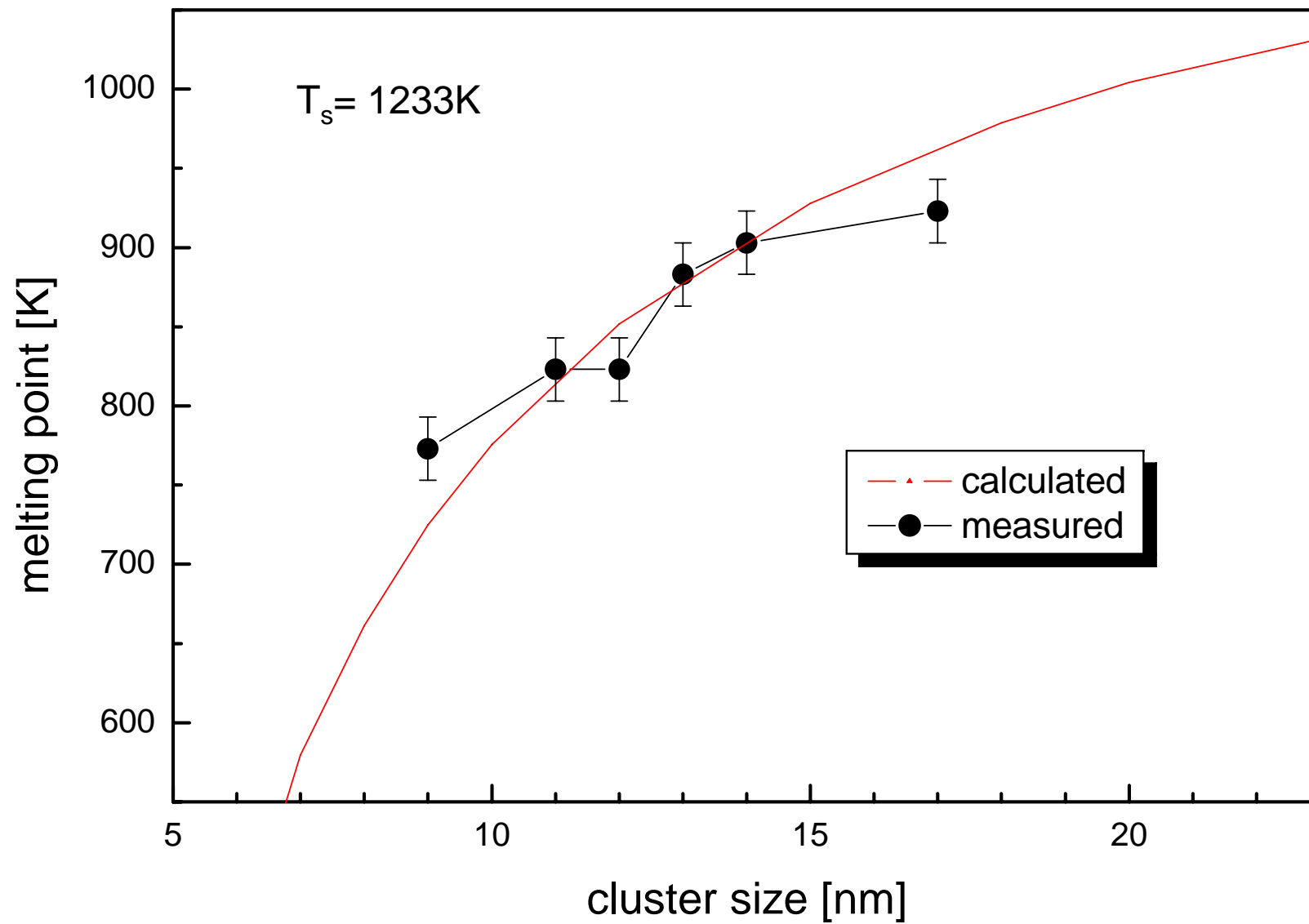
$$\frac{dp}{dT} = \frac{\Delta S}{\Delta T} \quad \longrightarrow \quad RT \ln \frac{p}{p_\infty} = \frac{\Delta H \cdot \Delta T}{T_\infty}$$

$$\frac{\Delta T}{T_\infty} = \frac{4 \cdot \sigma \cdot M}{\Delta H_\infty \cdot r \cdot \rho}$$

$$\Delta T = T_\infty - T_r$$

Ag cluster, peak (111), GID , with high temperature chamber HDK 2.4.





Zusammenfassung

Kombination von GIXD and XR: leistungsfähige Diagnostik von dünnen Schichten

Problem: GIXD nur für kristalline Proben

zerstörungsfrei

Nächste Vorhaben: insitu Untersuchungen von Plasma-Wand Prozessen:

- Danksagung
- Christoph Eggs
- Jens Klimke
- Hartmut Steffen
- Marion Quaas
- Shyjumon Ibrahimkutty

Ende